

Pairing 6D SCFTs

Peter R. Merks^a

^a*Department of Mathematics and Computer Science, Wesleyan University, Middletown CT, 06459*

E-mail: pmerks@wesleyan.edu

ABSTRACT: We study families of orbifolds underlying 6D SCFT F-theory models and find a novel pairing structure in the SCFT landscape. Inspection of the rational functions defining models with a common F-theory endpoint leads us naturally to pair them and uncover an extension to a larger combinatorial structure involving multi-family groupings. We investigate the correspondence of theories in grouped families via explicit computation of their gauge algebras. We find these typically match both in total number and rank structure with differences due to a fixed additional gauge summand. The underlying \mathbb{C}^2 orbifold pairing is distinct from the lattice/overlattice orbifold duality, the latter not being closed on the set of SCFT endpoints. Structural features of the endpoint collection including a canonical ordering are respected by this pairing. In a tower description of the endpoint landscape, repeated pairings induce an intricate combinatorial structure near the tower base which we partially characterize.

Contents

1	Introduction	1
2	An SCFT pairing	3
2.1	Discrete $U(2)$ gauge field and \mathbb{C}^2 orbifold overview	3
2.2	Defining the pairing	4
3	T^* paired gauge algebras	7
3.1	Gauge algebra counts for all T^* pairs	8
3.2	Comparison of T^* and dual-overlattice pairings	11
4	On 6D SCFT endpoint combinatorics	12
4.1	From relations to SCFT compatible orbifolds	13
4.2	Intermediate determinants and canonical bases	14
4.3	SCFT endpoint families and $PSL(2, p)$	18
5	Conclusions	19
A	Expression of discrete $U(2)$ subgroup generators from leads/tails	20
B	Miscellaneous tables, D-type endpoints	21
C	$n < 0$ extrapolated endpoints	23
D	Lower level endpoint pairing orbits	27

1 Introduction

Our focus here is the structure of 6D SCFT endpoint families as classified in [1]. We detail a pairing of these endpoints and make a few combinatorial observations concerning the rational functions determining these families. We will refer to this as a T^* pairing, owing to its description as a transposition in a certain grid arrangement of the permitted linear endpoints. Evidence that this pairing is natural includes an apparent relationship between the structure of gauge algebras in T^* paired families of SCFTs. The underlying orbifold pairs differ from the established lattice/overlattice \mathbb{C}^2 orbifold duality. These pairings are however rather closely related with a notable difference being that the overlattice duality is not closed on SCFT endpoints. An explanation of T^* pairing via a precise geometric duality between \mathbb{C}^2 orbifolds or a more elaborate geometric correspondence between paired families of Calabi-Yau (CY) threefolds remains to be found.

The continued fraction formulas defining endpoint families have several properties respected by T^* pairing. Through further inspection of these functions, we find that they have a simple combinatorial description. In other words, the rational functions that determine valid SCFT families arise from a small set of constraints.

More precisely, it was shown in [2] that all 6D SCFTs come in families with a structure consisting of 78 (infinite) families of linear endpoints, 4 (infinite) branching families (that we can regard as living inside the 78 families), and a handful of exceptional endpoints (corresponding to the Dynkin diagrams of the exceptional Lie groups). The linear endpoint families arrange into what we accordingly term *levels*, with each level consisting of 78 endpoints corresponding to unordered pairs of integers $1 \leq n, m \leq 12$. We find several relations obeyed by rational functions defining these endpoints including certain constraint equations. These provide a prescription for the collection of all such functions easily phrased as a requirement that, as fractional linear transformations, determinants must appear as the square of an integer $1 \leq k \leq 6$. Though an explanation why only these rational functions define the collection of SCFTs is still somewhat lacking, the integer parameters involved in previous endpoint family characterizations hence do have a comparatively parsimonious description with notable number theoretic properties. Amongst these are that the underlying constraints can be rephrased as those needed to regard these rational functions as projective fractional linear transformations over certain finite fields.

A simple but striking combinatorial observation concerning the established collection of rational functions defining 6D SCFT endpoints lies at the core of our investigation of T^* pairing. Certain orderings of endpoint families make clear that this collection exhibits an unexpected pairing phenomenon. Further inspection via gauge algebra families in each of the apparent pairs confirms that the pairing in question is reflected also at the level of gauge enhancements structure. We check the latter by explicit brute force comparison of the gauge algebras of 6D SCFTs in each endpoint family. We find that the paired endpoints in a fixed level have deep structural correspondences, typically manifesting as a difference by an overall gauge summand. Endpoint family degenerations occurring at small n leads T^* pairing to induce longer orbits that endow the SCFT landscape with a rich combinatorial structure described in Appendix D. The gauge enhancement structure correspondence on pairs links the number of SCFTs in each endpoint with the geometry of \mathbb{C}^2/Γ . Consequently, this may indicate a relationship between the structure in T^* paired sectors of CY threefold moduli space with the role of longer orbits arising from low level degenerations being of potential interest.

The remainder of this note is structured as follows. In Section 2, we review the \mathbb{C}^2 orbifolds underlying F-theory 6D SCFT models and detail canonical orderings of their families compatible with T^* pairing. Enhancement structure respected by T^* pairing is discussed in Section 3 where we also briefly discuss similarities of T^* pairing with N^* orbifold duality. Section 4 consists of several combinatorial observations concerning the rational functions defining endpoint families including relations obeyed by their integer parameters that respect T^* endpoint groupings and providing a partial fraction-intrinsic characterization of the permitted endpoint families. In Appendix A, we review an alternative condensed description of the 78 rational functions for permitted linear endpoint orbifold actions. We

extend parts of our discussion to D-type endpoints in Appendix B along with a few tables peripheral to our discussion. In Appendix C, we list negative level endpoint extrapolations. In Appendix D we detail all longer T^* induced orbits arising at low-level.

2 An SCFT pairing

2.1 Discrete $U(2)$ gauge field and \mathbb{C}^2 orbifold overview

Recall from [2] that the collection of linear endpoints occurring in infinite families can be expressed as $\alpha A_n \bar{\beta}$ for $\alpha, \bar{\beta} \in H := \{7, 6, 5, 4, 3, 24, 23, 223, 2223, 22223, \emptyset\}$, where $\bar{\beta}$ denotes the reverse of a string (e.g. for $\alpha = 23$, we have $\bar{\alpha} = 32$), \emptyset denotes the empty string, and A_n denotes a length n string $22 \cdots 2$. We will refer to the strings in H as leads/tails. Each linear endpoint has an associated orbifold $B \cong C^2/\Gamma$ with $\Gamma \subset U(2)$ a discrete $U(2)$ subgroup with generator

$$(z_1, z_2) \mapsto (z_1 e^{2\pi i \frac{1}{p}}, z_2 e^{2\pi i \frac{q}{p}}). \quad (2.1)$$

We denote the values of p, q which occur for the endpoint $\alpha A_n \bar{\beta}$ by $p(\alpha A_n \bar{\beta}), q(\alpha A_n \bar{\beta})$, respectively. We similarly define $\frac{p}{q}(\alpha A_n \bar{\beta})$ in the obvious way. The values of p, q here are determined by the Hirzebruch-Jung continued fraction obtained from the endpoint string $\gamma \sim m_1 \cdots m_r$ via

$$\begin{aligned} \frac{p}{q}(m_1, \dots, m_r) &= [m_1, \dots, m_r] \\ &= m_1 - \frac{1}{[m_2, \dots, m_r]} \\ &= m_1 - \frac{1}{m_2 - \frac{1}{\dots}} \\ &\qquad\qquad\qquad \dots \qquad\qquad\qquad \frac{1}{m_{n-1} - \frac{1}{m_n}} \end{aligned} \quad (2.2)$$

Related notions are treated in greater depth in earlier literature [3]. A few established observations we review for clarity are the following. The fraction p/q defines a lattice $\mathbb{Z}^2 + \mathbb{Z}(\frac{1}{p}, \frac{q}{p})$ whose convex hull of non-zero points in the first quadrant has boundary points we shall refer to as Newton L . Conversely, we can determine uniquely a string of curves from a given rational via a sequence of roundup operations. The invariant monomials $C[z_1, z_2]$ for the orbifold determined by p/q are generated by the overlattice dual $N^*(\gamma) \sim \tilde{m}_1, \dots, \tilde{m}_n$ corresponding to the fraction $\frac{p}{p-q}$. More precisely, we can read the generating invariant monomials from the numerators appearing in the overlattice dual endpoint Newton L boundary points when written with minimal common denominator. Note that even when γ is a 6D SCFT endpoint, $N^*(\gamma)$ may not be. For example, $\gamma \sim 3333$ has $N^*(\gamma) \sim 23332$ corresponding to an orbifold failing to support any valid 6D SCFT minimal resolution.

2.2 Defining the pairing

We begin by inspecting the values of n yielding roots of $p(\alpha A_n \beta)$ in the extrapolated $\frac{p}{q}(\alpha A_n \beta)$ values dating to [1, 2] which we take with a reordering displayed in Table 1 in terms of the level, n , rather than the total number of curves N in $\alpha A_n \beta$ as in [1, 2]. These roots correspond to a breakdown in the orbifold generator action upon extrapolating the continued fraction values for $p(\alpha A_n \beta)$ to $n = -2$. There are 2^5 preferred symmetric lead/tail orderings with all breakdowns falling on the 11×11 nonempty lead/tail block anti-diagonal. Table 1 gives the permitted $f(n)$ in one such ordering.

$\alpha \backslash \beta$	32222	3222	4	33	322	3	5	42	32	6	7	\emptyset
22223	$\frac{36n+96}{30n+79}$	$\frac{30n+79}{25n+65}$	$\frac{18n+45}{15n+37}$	$\frac{30n+67}{25n+55}$	$\frac{24n+50}{20n+41}$	$\frac{12n+28}{10n+23}$	$\frac{24n+62}{20n+51}$	$\frac{30n+73}{25n+60}$	$\frac{18n+39}{15n+32}$	$\frac{30n+61}{25n+50}$	$\frac{36n+72}{30n+59}$	$\frac{6n+11}{5n+9}$
2223	$\frac{30n+79}{24n+62}$	$\frac{25n+65}{20n+51}$	$\frac{15n+37}{12n+29}$	$\frac{25n+55}{20n+43}$	$\frac{20n+41}{16n+32}$	$\frac{10n+23}{8n+18}$	$\frac{20n+51}{16n+40}$	$\frac{25n+60}{20n+47}$	$\frac{15n+32}{12n+25}$	$\frac{25n+50}{20n+39}$	$\frac{30n+59}{24n+46}$	$\frac{5n+9}{4n+7}$
4	$\frac{18n+45}{12n+28}$	$\frac{15n+37}{10n+23}$	$\frac{9n+21}{6n+13}$	$\frac{15n+31}{10n+19}$	$\frac{12n+23}{8n+14}$	$\frac{6n+13}{4n+8}$	$\frac{12n+29}{8n+18}$	$\frac{15n+34}{10n+21}$	$\frac{9n+18}{6n+11}$	$\frac{15n+28}{10n+17}$	$\frac{18n+33}{12n+20}$	$\frac{3n+5}{2n+3}$
33	$\frac{30n+67}{18n+39}$	$\frac{25n+55}{15n+32}$	$\frac{15n+31}{9n+18}$	$\frac{25n+45}{15n+26}$	$\frac{20n+33}{12n+19}$	$\frac{10n+19}{6n+11}$	$\frac{20n+43}{12n+25}$	$\frac{25n+50}{15n+29}$	$\frac{15n+26}{9n+15}$	$\frac{25n+40}{15n+23}$	$\frac{30n+47}{18n+27}$	$\frac{5n+7}{3n+4}$
223	$\frac{24n+50}{6n+11}$	$\frac{20n+41}{5n+9}$	$\frac{12n+23}{3n+5}$	$\frac{20n+33}{5n+7}$	$\frac{16n+24}{4n+5}$	$\frac{8n+14}{2n+3}$	$\frac{16n+32}{4n+7}$	$\frac{20n+37}{5n+8}$	$\frac{12n+19}{3n+4}$	$\frac{20n+29}{5n+6}$	$\frac{24n+34}{6n+7}$	$\frac{4n+5}{n+1}$
3	$\frac{12n+28}{6n+11}$	$\frac{10n+23}{5n+9}$	$\frac{6n+13}{3n+5}$	$\frac{10n+19}{5n+7}$	$\frac{8n+14}{4n+5}$	$\frac{4n+8}{2n+3}$	$\frac{8n+18}{4n+7}$	$\frac{10n+21}{5n+8}$	$\frac{6n+11}{3n+4}$	$\frac{10n+17}{5n+6}$	$\frac{12n+20}{6n+7}$	$\frac{2n+3}{n+1}$
5	$\frac{24n+62}{18n+45}$	$\frac{20n+51}{15n+37}$	$\frac{12n+29}{9n+21}$	$\frac{20n+43}{15n+31}$	$\frac{16n+32}{12n+23}$	$\frac{8n+18}{6n+13}$	$\frac{16n+40}{12n+29}$	$\frac{20n+47}{15n+34}$	$\frac{12n+25}{9n+18}$	$\frac{20n+39}{15n+28}$	$\frac{24n+46}{18n+33}$	$\frac{4n+7}{3n+5}$
24	$\frac{30n+73}{12n+28}$	$\frac{25n+60}{10n+23}$	$\frac{15n+34}{6n+13}$	$\frac{25n+50}{10n+19}$	$\frac{20n+37}{8n+14}$	$\frac{10n+21}{4n+8}$	$\frac{20n+47}{8n+18}$	$\frac{25n+55}{10n+21}$	$\frac{15n+29}{6n+11}$	$\frac{25n+45}{10n+17}$	$\frac{30n+53}{12n+20}$	$\frac{5n+8}{2n+3}$
23	$\frac{18n+39}{6n+11}$	$\frac{15n+32}{5n+9}$	$\frac{9n+18}{3n+5}$	$\frac{15n+26}{5n+7}$	$\frac{12n+19}{4n+5}$	$\frac{6n+11}{2n+3}$	$\frac{12n+25}{4n+7}$	$\frac{15n+29}{5n+8}$	$\frac{9n+15}{3n+4}$	$\frac{15n+23}{5n+6}$	$\frac{18n+27}{6n+7}$	$\frac{3n+4}{n+1}$
6	$\frac{30n+61}{6n+11}$	$\frac{25n+50}{5n+9}$	$\frac{15n+28}{3n+5}$	$\frac{25n+40}{5n+7}$	$\frac{20n+29}{4n+5}$	$\frac{10n+17}{2n+3}$	$\frac{20n+39}{4n+7}$	$\frac{25n+45}{5n+8}$	$\frac{15n+23}{3n+4}$	$\frac{25n+35}{5n+6}$	$\frac{30n+41}{6n+7}$	$\frac{5n+6}{n+1}$
7	$\frac{36n+72}{6n+11}$	$\frac{30n+59}{5n+9}$	$\frac{18n+33}{3n+5}$	$\frac{30n+47}{5n+7}$	$\frac{24n+34}{4n+5}$	$\frac{12n+20}{2n+3}$	$\frac{24n+46}{4n+7}$	$\frac{30n+53}{5n+8}$	$\frac{18n+27}{3n+4}$	$\frac{30n+41}{5n+6}$	$\frac{36n+48}{6n+7}$	$\frac{6n+7}{n+1}$
\emptyset	$\frac{6n+11}{6n+5}$	$\frac{5n+9}{5n+4}$	$\frac{3n+5}{3n+2}$	$\frac{5n+7}{5n+2}$	$\frac{4n+5}{4n+1}$	$\frac{2n+3}{2n+1}$	$\frac{4n+7}{4n+3}$	$\frac{5n+8}{5n+3}$	$\frac{3n+4}{3n+1}$	$\frac{5n+6}{5n+1}$	$\frac{6n+7}{6n+1}$	$\frac{n+1}{n}$

Table 1: Continued fraction values $\frac{p}{q}$ for linear endpoints of the form $\alpha A_n \beta$.

The obstruction to $n = -2$ extrapolations in certain endpoint families owes to a root of $p(n)$ (rather than merely non-existence of an SCFT endpoint with specified p/q values). Each integer root for any of the expressions $\frac{p}{q}(\alpha A_n \beta)$ (as in Table 1) appears at $n = -2$ with one exception at $n = -1$ for the empty lead/tail endpoint that is naturally moved to level $n = -2$.¹ We compute the negated roots of $p(\alpha A_n \beta)$ in n that we will refer to as p -roots. These values appear in Table 21 for completeness. Upon reduction modulo 1, a reflection symmetry about the 11×11 anti-diagonal becomes apparent as illustrated in Table 2. The large groupings of matching signs is unique to this among the 2^5 orderings under consideration.

¹We can consider $n = 0$ to correspond to the minimal non-empty endpoints at that level of the form $\alpha A_n \beta$. This reindexing is natural with respect to canonical base truncation induced orderings and level indexing.

$\alpha \backslash \beta$	7	6	5	4	42	3	33	32	322	3222	32222	2
7	$-\frac{1}{3}$	$-\frac{11}{30}$	$-\frac{5}{12}$	$\frac{1}{2}$	$\frac{13}{30}$	$\frac{1}{3}$	$\frac{7}{30}$	$\frac{1}{6}$	$\frac{1}{12}$	$\frac{1}{30}$	0	$-\frac{1}{6}$
6	$-\frac{11}{30}$	$-\frac{2}{5}$	$-\frac{9}{20}$	$\frac{7}{15}$	$\frac{2}{5}$	$\frac{3}{10}$	$\frac{1}{5}$	$\frac{2}{15}$	$\frac{1}{20}$	0	$-\frac{1}{30}$	$-\frac{1}{5}$
5	$-\frac{5}{12}$	$-\frac{9}{20}$	$\frac{1}{2}$	$\frac{5}{12}$	$\frac{7}{20}$	$\frac{1}{4}$	$\frac{3}{20}$	$\frac{1}{12}$	0	$-\frac{1}{20}$	$-\frac{1}{12}$	$-\frac{1}{4}$
4	$\frac{1}{2}$	$\frac{7}{15}$	$\frac{5}{12}$	$\frac{1}{3}$	$\frac{4}{15}$	$\frac{1}{6}$	$\frac{1}{15}$	0	$-\frac{1}{12}$	$-\frac{2}{15}$	$-\frac{1}{6}$	$-\frac{1}{3}$
24	$\frac{13}{30}$	$\frac{2}{5}$	$\frac{7}{20}$	$\frac{4}{15}$	$\frac{1}{5}$	$\frac{1}{10}$	0	$-\frac{1}{15}$	$-\frac{3}{20}$	$-\frac{1}{5}$	$-\frac{7}{30}$	$-\frac{2}{5}$
3	$\frac{1}{3}$	$\frac{3}{10}$	$\frac{1}{4}$	$\frac{1}{6}$	$\frac{1}{10}$	0	$-\frac{1}{10}$	$-\frac{1}{6}$	$-\frac{1}{4}$	$-\frac{3}{10}$	$-\frac{1}{3}$	$\frac{1}{2}$
33	$\frac{7}{30}$	$\frac{1}{5}$	$\frac{3}{20}$	$\frac{1}{15}$	0	$-\frac{1}{10}$	$-\frac{1}{5}$	$-\frac{4}{15}$	$-\frac{7}{20}$	$-\frac{2}{5}$	$-\frac{13}{30}$	$\frac{2}{5}$
23	$\frac{1}{6}$	$\frac{2}{15}$	$\frac{1}{12}$	0	$-\frac{1}{15}$	$-\frac{1}{6}$	$-\frac{4}{15}$	$-\frac{1}{3}$	$-\frac{5}{12}$	$-\frac{7}{15}$	$\frac{1}{2}$	$\frac{1}{3}$
223	$\frac{1}{12}$	$\frac{1}{20}$	0	$-\frac{1}{12}$	$-\frac{3}{20}$	$-\frac{1}{4}$	$-\frac{7}{20}$	$-\frac{5}{12}$	$\frac{1}{2}$	$\frac{9}{20}$	$\frac{5}{12}$	$\frac{1}{4}$
2223	$\frac{1}{30}$	0	$-\frac{1}{20}$	$-\frac{2}{15}$	$-\frac{1}{5}$	$-\frac{3}{10}$	$-\frac{2}{5}$	$-\frac{7}{15}$	$\frac{9}{20}$	$\frac{2}{5}$	$\frac{11}{30}$	$\frac{1}{5}$
22223	0	$-\frac{1}{30}$	$-\frac{1}{12}$	$-\frac{1}{6}$	$-\frac{7}{30}$	$-\frac{1}{3}$	$-\frac{13}{30}$	$\frac{1}{2}$	$\frac{5}{12}$	$\frac{11}{30}$	$\frac{1}{3}$	$\frac{1}{6}$
2	$-\frac{1}{6}$	$-\frac{1}{5}$	$-\frac{1}{4}$	$-\frac{1}{3}$	$-\frac{2}{5}$	$\frac{1}{2}$	$\frac{2}{5}$	$\frac{1}{3}$	$\frac{1}{4}$	$\frac{1}{5}$	$\frac{1}{6}$	0

Table 2: p roots modulo 1 with leads in canonical base truncation induced order.

A corresponding pairing of lead strings in the final column about the 3-lead row entry is also visible. Swaps of these 5 pairs generate the 2^5 base changes preserving the 11×11 anti-diagonal. Note that the $p(n)$ -roots (and similarly $q(n)$ -roots) modulo 1 are natural invariants of $f(n)$ since they are independent of the n -level shift and the rescaling $(p, q) \mapsto (ap, aq)$. In other words, for $f_{\alpha, \beta}(n) := f(n)$ and $\tilde{f}_k(n) := f(n+k)$ with $k \in \mathbb{Z}_{\geq 0}$ we have

$$\left(f(s) = 0 \quad \text{and} \quad \tilde{f}_k(s') = 0 \right) \implies s \equiv s' \pmod{1}. \quad (2.3)$$

These symmetries yield a pairing of endpoints of the form $\alpha A_n \beta$ provided we regard the 6 fixed endpoint orbifold isomorphism classes as paired to themselves (i.e. self-dual). The induced map on mixed leads follows from the lead pairing, thus allowing it to be summarized via Figure 1. We observe that those leads playing a central role upon the introduction of frozen divisors [4, 5] also play an exceptional role in T^* pairing, e.g. the self-dual leads 2 and 3 and the T^* lead pair $23 \leftrightarrow 4$.

Each of the rational functions defining an endpoint family takes the form

$$f(n) = \frac{k_u n + r_u}{k_l n + r_l}. \quad (2.4)$$

We define the *fraction determinant* of $f(n)$ as

$$\det(f(n)) := (k_u \cdot r_l - k_l \cdot r_u), \quad (2.5)$$

noting the invariance under shifts $n \mapsto \tilde{n} := n+k$ inducing $f(n) \mapsto \tilde{f}(\tilde{n})$ with $f(n), \tilde{f}(\tilde{n})$

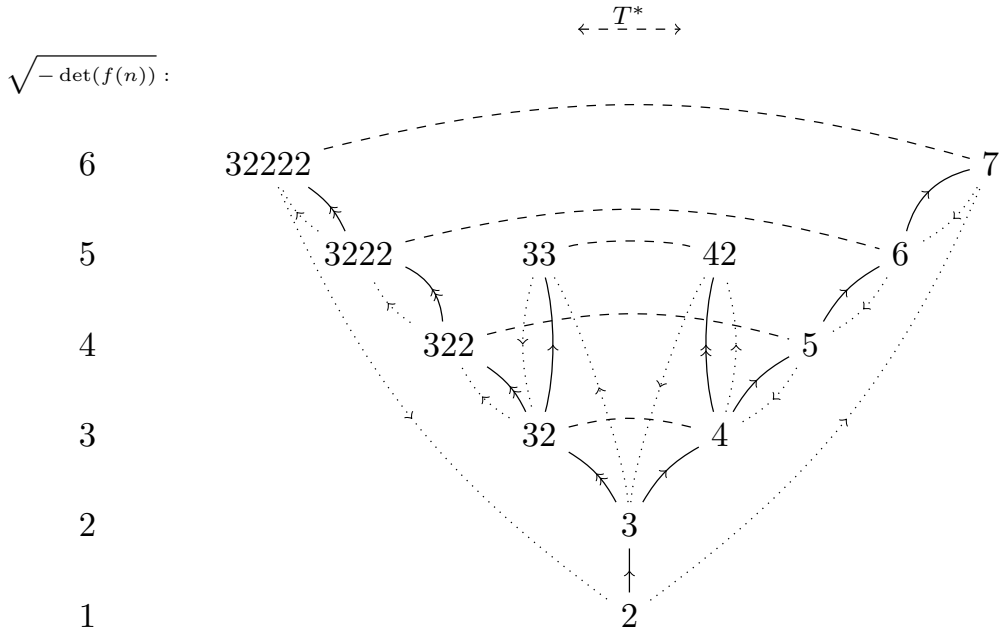


Figure 1: T^* lead relations. Nearest canonical base representative truncations are indicated by dotted arrows, T^* pairings by dashed arrows, and transitions from blowing up a point on the right-most curve and truncating the resulting -1 curve by solid single arrows. Solid double arrows indicate maps resulting from inclusion in a longer base with a rightmost -1 curve, blowing up this curve and truncating the resulting -1 curve.

yielding equivalent sequences in \mathbb{Q} . The value of $\det(f(n))$ is constant on the columns of Table 1 with values appearing in Table 3. Note that $-\det(f(n)) \in \{k^2 : 1 \leq k \leq 6\}$ with $f(n)$ obeying

$$-\det(f(n)) = \gcd(k_u, k_l)^2, \quad (2.6)$$

hence requiring that $\gcd(k_u, k_l)$ is also α invariant.

$\beta :$	32222	3222	4	33	322	3	5	42	32	6	7	\emptyset
$-\det(f(\alpha A_n \beta)):$	6^2	5^2	3^2	5^2	4^2	2^2	4^2	5^2	3^2	5^2	6^2	1

Table 3: The (α independent) values of $-\det(f(\alpha A_n \beta))$.

We can reorder the leads and tails separately to express T^* pairing for leads on the same footing in a grid as other endpoints. Column swaps allow placement of all zeros on the diagonal. Further swaps of (non-matching) tails subsequently groups identical denominators with first row numerators descending within each group. The resulting roots of $p(\alpha A_n \beta)$ appear in Table 21. This ordering makes apparent that T^* pairing respects the block diagonal grouping apparent in Table 14 of the determinant action $\det : \Gamma \rightarrow U(1)$ originally observed in [2] that we discuss further in Section 4.2. Numerators within com-

mon denominator groups move by uniform jumps in each row and column as we approach the diagonal in Table 21. Our ‘ T^* ’ notation owes to the correspondence of the pairing with transposition of the resulting grid. Though the explicit pairing is succinctly captured by Figure 1, we include an explicit listing in Table 20 with cases permitting infinitely many enhancements indicated.

3 T^* paired gauge algebras

Here we focus on the relationship between gauge algebras within T^* paired endpoints. Our study will be restricted to the non-branching bases in each endpoint pair for computational ease. We compute the gauge algebras on these bases in T^* paired endpoints for a fixed n and find that endpoint pairs often exhibit a pattern of degeneration towards matching at sufficiently large n .

We will refer to the number of gauge algebras supported on the linear quivers in an endpoint α as $N_a(\alpha)$. As we move up the tower of levels, endpoint pairs $\alpha \leftrightarrow \beta$ have $N_a(\alpha), N_a(\beta)$ that generally stabilize to achieve near, and typically exact, matching. For example, consider the T^* paired family, namely $22223A_n \leftrightarrow A_n7$. Values of N_a in this case appear in Table 4. They converge to match exactly for $4 \leq n \leq 10$ (and conjecturally $n \geq 11$). The structure of the algebras on each side of this pairing at $n = 10$ is identical up to a uniform addition of a $A_1^2 \oplus \mathfrak{f}_4 \oplus \mathfrak{g}_2^2$ gauge summand as shown in Table 8.

n :	# Gauge algs. on $\{22223A_n, -A_n7\}$:
1	{193,30}
2	{128,35}
3	{71,37}
4	{38,38}
5	{38,38}
6	{38,38}
7	{38,38}
8	{38,38}
9	{38,38}
10	{38,38}

Table 4: Number of gauge algebras on linear bases in the endpoint pairs $22223A_n \leftrightarrow A_n7$ for various n values. For fixed $n \geq 4$, the T^* paired gauge algebra lists differ by a $A_1^2 \oplus \mathfrak{f}_4 \oplus \mathfrak{g}_2^2$ summand.

A second case exhibiting similar behavior appears in Table 5 where rank pairing is instead due to uniform addition of \mathfrak{f}_4 summand. Though frequent, this type of uniform difference pairing does not hold in all cases. Paired sets of enhancements do appear to have similar structure, but can be more involved. For example, Table 7 illustrates an additional gauge summand is not always responsible for enhancement count matching.

The general correspondence appears to be more subtle in two ways. First, a rich paired combinatorial enhancement structure typically holds for small n before a tight correspondence arises. Whether this owes to T^* pairing corresponding to a deeper duality of field

Gauge Alg. \mathfrak{g}_a on $\alpha \sim 3A_{10}33$	Gauge Alg. \mathfrak{g}_b on $T^*\alpha \sim 3A_{10}42$	Rank(\mathfrak{g}_a)	Rank(\mathfrak{g}_b)
$A_1^{22} \oplus A_2 \oplus e_6 \oplus e_8^{11} \oplus f_4^{12} \oplus g_2^{22}$	$A_1^{22} \oplus A_2 \oplus e_6 \oplus e_8^{11} \oplus f_4^{11} \oplus g_2^{22}$	202	198
$A_1^{23} \oplus e_7 \oplus e_8^{11} \oplus f_4^{12} \oplus g_2^{23}$	$A_1^{23} \oplus A_2 \oplus e_6 \oplus e_8^{11} \oplus f_4^{11} \oplus g_2^{22}$	210	206
$A_1^{23} \oplus e_8^{12} \oplus f_4^{12} \oplus g_2^{23}$	$A_1^{23} \oplus e_7 \oplus e_8^{11} \oplus f_4^{11} \oplus g_2^{23}$	212	208
$A_1^{24} \oplus e_8^{12} \oplus f_4^{12} \oplus g_2^{23}$	$A_1^{23} \oplus e_8^{12} \oplus f_4^{11} \oplus g_2^{23}$	213	209
$A_1^{25} \oplus e_8^{12} \oplus f_4^{12} \oplus g_2^{23}$	$A_1^{24} \oplus e_8^{12} \oplus f_4^{11} \oplus g_2^{23}$	214	210
$A_1^{24} \oplus e_8^{12} \oplus f_4^{12} \oplus g_2^{24}$	$A_1^{25} \oplus e_8^{12} \oplus f_4^{11} \oplus g_2^{23}$	215	211
$A_1^{24} \oplus A_2 \oplus e_8^{12} \oplus f_4^{12} \oplus g_2^{23}$	$A_1^{24} \oplus e_8^{12} \oplus f_4^{11} \oplus g_2^{24}$	216	212
	$A_1^{24} \oplus A_2 \oplus e_8^{12} \oplus f_4^{11} \oplus g_2^{23}$	216	212

Table 5: Gauge algebras and ranks for all linear quiver based theories in each endpoint of the $n = 10$ pair $3A_{10}33 \leftrightarrow 3A_{10}42$. Difference by an f_4 summand accounts for the uniform rank 4 differences.

theories and/or CY moduli space sectors remains unclear. Evidence against fixed $p(n)$ singularity behavior being responsible for the observed gauge algebra family pairing phenomena is provided by drastically different enhancement counts in non T^* paired families sharing p roots modulo 1. Second, a few branching bases are in some cases allowed. We do not include branching bases in our computations of the permitted gauge enhancements for computational ease at the cost of introducing typically minor paired enhancement count mismatches even for large n . Chains of pairings that arise due to endpoint family degenerations for small n are discussed separately in Appendix D.

Endpoints α with $N_a(\alpha) = \infty$ at level $n = 0$ are identified with two exceptions eliminated provided we pair entire endpoint families across levels. One of these is the pairing $33A_n \leftrightarrow 24A_n$ which has 33 easily seen to hold infinitely many enhancements (since its minimal resolution, namely 414 permits infinitely many enhancements) while 24 supports only finitely many at $n = 0$; this count however becomes infinite at $n = -1$. (Interestingly, $N_a(24) \approx 216$, is perhaps the largest among finite N_a at $n = 0$.)²

3.1 Gauge algebra counts for all T^* pairs

To confirm that T^* pairing yields a correspondence between SCFT gauge algebras in of T^* paired endpoints more generally, we focus our attention on these pairs at $n = 10$. This value is large enough to avoid endpoint family mixing which may obscure N_a matching and reduce the role of branching bases that we wish to discard for computational simplicity. Note that matching level n pairs appears to be more natural than pairing endpoints with the same total number N of curves for several reasons. First, there is much closer matching of n -level pair algebra counts versus those for N -level pairs. Second, the correspondence with N^* duality appears to closely resemble T^* pairings at fixed n . Finally, the Section 2 examination of n -level expressions rather than those for N -level yields a uniform p singularity anti-diagonal of -2 .

²To confirm that the endpoints 5, 6, 322 and 3222 have $N_a = \infty$, two approaches are helpful. For 5 and 6, we can compare to the “long-bases” Appendix B of [6] (in particular B.22) to find infinitely many distinctly gauged bases blow down to 6 with 5 following after decorating by a rightmost -1 curve. For 322 and 3222, we can blow up to obtain (1)4141... with $N_a = \infty$.

Gauge Alg. \mathfrak{g}_a on $\alpha \sim A_43A_{10}$	Gauge Alg. \mathfrak{g}_b on $T^*\alpha \sim A_{10}7$	Rank(\mathfrak{g}_a)	Rank(\mathfrak{g}_b)
$A_1^{16} \oplus e_8^7 \oplus f_4^8 \oplus g_2^{16}$	$A_1^{14} \oplus e_8^7 \oplus f_4^7 \oplus g_2^{14}$	136	126
$A_1^{18} \oplus e_8^8 \oplus f_4^9 \oplus g_2^{18}$	$A_1^{16} \oplus e_8^8 \oplus f_4^8 \oplus g_2^{16}$	154	144
$A_1^{20} \oplus B_3 \oplus e_7 \oplus e_8^8 \oplus f_4^9 \oplus g_2^{18}$	$A_1^{18} \oplus B_3 \oplus e_7 \oplus e_8^8 \oplus f_4^8 \oplus g_2^{16}$	166	156
$A_1^{19} \oplus e_8^9 \oplus f_4^{10} \oplus g_2^{20}$	$A_1^{17} \oplus e_8^9 \oplus f_4^9 \oplus g_2^{18}$	171	161
$A_1^{19} \oplus A_2 \oplus e_8^9 \oplus f_4^{10} \oplus g_2^{19}$	$A_1^{17} \oplus A_2 \oplus e_8^9 \oplus f_4^9 \oplus g_2^{17}$	171	161
$A_1^{19} \oplus A_2^2 \oplus e_6 \oplus e_8^9 \oplus f_4^{10} \oplus g_2^{21}$	$A_1^{17} \oplus A_2^2 \oplus e_6 \oplus e_8^9 \oplus f_4^9 \oplus g_2^{19}$	179	169
$A_1^{21} \oplus e_7 \oplus e_8^9 \oplus f_4^{10} \oplus g_2^{21}$	$A_1^{19} \oplus e_7 \oplus e_8^9 \oplus f_4^9 \oplus g_2^{19}$	182	172
$A_1^{21} \oplus B_3 \oplus e_7 \oplus e_8^9 \oplus f_4^{10} \oplus g_2^{20}$	$A_1^{19} \oplus B_3 \oplus e_7 \oplus e_8^9 \oplus f_4^9 \oplus g_2^{18}$	183	173
$A_1^{21} \oplus e_8^{10} \oplus f_4^{10} \oplus g_2^{21}$	$A_1^{19} \oplus e_8^{10} \oplus f_4^9 \oplus g_2^{19}$	183	173
$A_1^{21} \oplus e_8^{10} \oplus f_4^{11} \oplus g_2^{21}$	$A_1^{19} \oplus e_8^{10} \oplus f_4^{10} \oplus g_2^{19}$	187	177
$A_1^{21} \oplus D_4 \oplus e_8^{10} \oplus f_4^{10} \oplus g_2^{21}$	$A_1^{19} \oplus D_4 \oplus e_8^{10} \oplus f_4^9 \oplus g_2^{19}$	187	177
$A_1^{21} \oplus D_4^2 \oplus e_8^{10} \oplus f_4^{10} \oplus g_2^{21}$	$A_1^{19} \oplus D_4^2 \oplus e_8^{10} \oplus f_4^9 \oplus g_2^{19}$	191	181
$A_1^{21} \oplus e_8^{10} \oplus f_4^{12} \oplus g_2^{22}$	$A_1^{19} \oplus e_8^{10} \oplus f_4^{11} \oplus g_2^{20}$	193	183
$A_1^{21} \oplus A_2 \oplus e_8^{10} \oplus f_4^{12} \oplus g_2^{21}$	$A_1^{19} \oplus A_2 \oplus e_8^{10} \oplus f_4^{11} \oplus g_2^{19}$	193	183
$A_1^{21} \oplus A_2 \oplus e_6 \oplus e_8^{10} \oplus f_4^{11} \oplus g_2^{21}$	$A_1^{19} \oplus A_2 \oplus e_6 \oplus e_8^{10} \oplus f_4^{10} \oplus g_2^{19}$	195	185
$A_1^{22} \oplus e_6 \oplus e_8^{10} \oplus f_4^{11} \oplus g_2^{22}$	$A_1^{20} \oplus e_6 \oplus e_8^{10} \oplus f_4^{10} \oplus g_2^{20}$	196	186
$A_1^{22} \oplus e_7 \oplus e_8^{10} \oplus f_4^{11} \oplus g_2^{22}$	$A_1^{20} \oplus e_7 \oplus e_8^{10} \oplus f_4^{10} \oplus g_2^{20}$	197	187
$A_1^{23} \oplus e_7 \oplus e_8^{10} \oplus f_4^{11} \oplus g_2^{22}$	$A_1^{21} \oplus e_7 \oplus e_8^{10} \oplus f_4^{10} \oplus g_2^{20}$	198	188
$A_1^{22} \oplus e_8^{11} \oplus f_4^{11} \oplus g_2^{22}$	$A_1^{20} \oplus e_8^{11} \oplus f_4^{10} \oplus g_2^{20}$	198	188
$A_1^{23} \oplus e_8^{11} \oplus f_4^{11} \oplus g_2^{22}$	$A_1^{21} \oplus e_8^{11} \oplus f_4^{10} \oplus g_2^{20}$	199	189
$A_1^{24} \oplus e_8^{11} \oplus f_4^{11} \oplus g_2^{22}$	$A_1^{22} \oplus e_8^{11} \oplus f_4^{10} \oplus g_2^{20}$	200	190
$A_1^{23} \oplus e_8^{11} \oplus f_4^{11} \oplus g_2^{23}$	$A_1^{21} \oplus e_8^{11} \oplus f_4^{10} \oplus g_2^{21}$	201	191
$A_1^{23} \oplus A_2 \oplus e_8^{11} \oplus f_4^{11} \oplus g_2^{22}$	$A_1^{21} \oplus A_2 \oplus e_8^{11} \oplus f_4^{10} \oplus g_2^{20}$	201	191
$A_1^{25} \oplus e_8^{11} \oplus f_4^{11} \oplus g_2^{22}$	$A_1^{23} \oplus e_8^{11} \oplus f_4^{10} \oplus g_2^{20}$	201	191
$A_1^{24} \oplus e_8^{11} \oplus f_4^{11} \oplus g_2^{23}$	$A_1^{22} \oplus e_8^{11} \oplus f_4^{10} \oplus g_2^{21}$	202	192
$A_1^{24} \oplus A_2 \oplus e_8^{11} \oplus f_4^{11} \oplus g_2^{22}$	$A_1^{22} \oplus A_2 \oplus e_8^{11} \oplus f_4^{10} \oplus g_2^{20}$	202	192
$A_1^{23} \oplus e_8^{11} \oplus f_4^{11} \oplus g_2^{24}$	$A_1^{21} \oplus e_8^{11} \oplus f_4^{10} \oplus g_2^{22}$	203	193
$A_1^{23} \oplus A_2 \oplus e_8^{11} \oplus f_4^{11} \oplus g_2^{23}$	$A_1^{21} \oplus A_2 \oplus e_8^{11} \oplus f_4^{10} \oplus g_2^{21}$	203	193
$A_1^{23} \oplus A_2^2 \oplus e_8^{11} \oplus f_4^{11} \oplus g_2^{22}$	$A_1^{21} \oplus A_2^2 \oplus e_8^{11} \oplus f_4^{10} \oplus g_2^{20}$	203	193
$A_1^{23} \oplus B_3 \oplus e_8^{11} \oplus f_4^{11} \oplus g_2^{23}$	$A_1^{21} \oplus B_3 \oplus e_8^{11} \oplus f_4^{10} \oplus g_2^{21}$	204	194
$A_1^{23} \oplus A_2 \oplus A_3 \oplus e_8^{11} \oplus f_4^{11} \oplus g_2^{22}$	$A_1^{21} \oplus A_2 \oplus A_3 \oplus e_8^{11} \oplus f_4^{10} \oplus g_2^{20}$	204	194
$A_1^{23} \oplus e_8^{11} \oplus f_4^{12} \oplus g_2^{23}$	$A_1^{21} \oplus e_8^{11} \oplus f_4^{11} \oplus g_2^{21}$	205	195
$A_1^{23} \oplus D_4 \oplus e_8^{11} \oplus f_4^{11} \oplus g_2^{23}$	$A_1^{21} \oplus D_4 \oplus e_8^{11} \oplus f_4^{10} \oplus g_2^{21}$	205	195
$A_1^{23} \oplus B_4 \oplus e_8^{11} \oplus f_4^{11} \oplus g_2^{23}$	$A_1^{21} \oplus B_4 \oplus e_8^{11} \oplus f_4^{10} \oplus g_2^{21}$	205	195
$A_1^{24} \oplus e_8^{11} \oplus f_4^{12} \oplus g_2^{23}$	$A_1^{22} \oplus e_8^{11} \oplus f_4^{11} \oplus g_2^{21}$	206	196
$A_1^{23} \oplus e_8^{11} \oplus f_4^{12} \oplus g_2^{24}$	$A_1^{21} \oplus e_8^{11} \oplus f_4^{11} \oplus g_2^{22}$	207	197
$A_1^{23} \oplus A_2 \oplus e_8^{11} \oplus f_4^{12} \oplus g_2^{23}$	$A_1^{21} \oplus A_2 \oplus e_8^{11} \oplus f_4^{11} \oplus g_2^{21}$	207	197
$A_1^{24} \oplus e_8^{11} \oplus f_4^{12} \oplus g_2^{24}$	$A_1^{22} \oplus e_8^{11} \oplus f_4^{11} \oplus g_2^{22}$	208	198

Table 6: Gauge algebras and ranks for the theories in each endpoint of the $n = 10$ pair $A_43A_{10} \leftrightarrow A_{10}7$. Difference by an $A_1^2 \oplus \mathfrak{f}_4 \oplus \mathfrak{g}_2^2$ summand accounts for the uniform rank 10 differences.

Gauge Alg. \mathfrak{g}_a on $\alpha \sim 4A_{10}7$	Gauge Alg. \mathfrak{g}_b on $T^*\alpha \sim A_43A_{10}32$	Rank(\mathfrak{g}_a)	Rank(\mathfrak{g}_b)
$A_1^{20} \oplus e_7 \oplus e_8^{10} \oplus f_4^{10} \oplus g_2^{20}$	$A_1^{23} \oplus e_8^{11} \oplus f_4^{11} \oplus g_2^{23}$	187	201
$A_1^{20} \oplus e_8^{11} \oplus f_4^{10} \oplus g_2^{20}$	$A_1^{23} \oplus e_8^{11} \oplus f_4^{12} \oplus g_2^{23}$	188	205
$A_1^{21} \oplus e_8^{11} \oplus f_4^{10} \oplus g_2^{20}$	$A_1^{23} \oplus D_4 \oplus e_8^{11} \oplus f_4^{11} \oplus g_2^{23}$	189	205

Table 7: Gauge algebras and ranks for the theories in each endpoint of the $n = 10$ pair $4A_{10}7 \leftrightarrow A_43A_{10}32$. Here gauge algebra pairs do not differ by a uniform factor.

The N_a counts for all T^* pairs at $n = 10$ appear as Table 8. We determine $N_a(\alpha)$ values by explicit computation of the permitted gauge algebras using the ancillary code of [7]. This entails first computing all bases in each endpoint and decorating their curves with any globally compatible gauge summands. These results rely in some cases on conjectural existence claims that may also be partly responsible for the minority of cases exhibiting N_a mismatches even at large n .

End-pair	# Enhancements
{22223 A_{10} 32222, 7 A_{10} 7}	{1,1}
{22223 A_{10} 3222, 6 A_{10} 7}	{1,1}
{22223 A_{10} 33, 24 A_{10} 7}	{1,1}
{22223 A_{10} 42, 33 A_{10} 7}	{1,1}
{22223 A_{10} 6, 2223 A_{10} 7}	{1,1}
{22223 A_{10} 322, 5 A_{10} 7}	{2,1}
{22223 A_{10} 5, 223 A_{10} 7}	{1,2}
{22223 A_{10} 4, 23 A_{10} 7}	{3,3}
{22223 A_{10} 3, 3 A_{10} 7}	{8,8}
{22223 A_{10} 32, 4 A_{10} 7}	{3,3}
{22223 A_{10} -, - A_{10} 7}	{38,38}
{6 A_{10} 6, 2223 A_{10} 3222}	{1,1}
{6 A_{10} 33, 24 A_{10} 3222}	{1,1}
{6 A_{10} 42, 33 A_{10} 3222}	{1,1}
{6 A_{10} 322, 5 A_{10} 3222}	{2,1}
{6 A_{10} 5, 223 A_{10} 3222}	{1,2}
{6 A_{10} 4, 23 A_{10} 3222}	{3,3}
{6 A_{10} 3, 3 A_{10} 3222}	{8,8}
{6 A_{10} 32, 4 A_{10} 3222}	{3,3}
{6 A_{10} -, - A_{10} 3222}	{38,38}
{24 A_{10} 42, 33 A_{10} 33}	{1,1}
{24 A_{10} 322, 5 A_{10} 33}	{2,1}
{24 A_{10} 5, 223 A_{10} 33}	{1,2}
{24 A_{10} 4, 23 A_{10} 33}	{3,3}
{24 A_{10} 3, 3 A_{10} 33}	{8,8}
{24 A_{10} 32, 4 A_{10} 33}	{3,3}
{24 A_{10} -, - A_{10} 33}	{38,38}
{5 A_{10} 5, 223 A_{10} 322}	{2,4}
{5 A_{10} 4, 23 A_{10} 322}	{4,8}
{5 A_6 3, 3 A_6 322}	{12,19}
{5 A_6 32, 4 A_6 322}	{5,7}
{5 A_6 -, - A_6 322}	{64,95}
{23 A_6 32, 4 A_6 4}	{10,8}
{23 A_6 3, 3 A_6 4}	{34,26}
{23 A_6 -, - A_6 4}	{168,143}

Table 8: Number of gauge algebras arising in paired endpoints. Each non-self-dual endpoint family pair appears once. The first grouping gives values at $n = 10$, while the second is listed for $n = 5$ for computational ease.

Groupings of T^* pairs which have common N_a values are evident. Invariants determined directly from permitted $f(n)$ make clear precisely which endpoint pairs naturally arrange into groups with (near) N_a agreement and are detailed in Section 4. This appears to suggest that T^* pairing may be one of a more involved collection of operations with

orbits consisting of corresponding SCFT structures.

3.2 Comparison of T^* and dual-overlattice pairings

We now turn to detail the distinction between T^* and N^* orbifold pairings. The latter pairs the orbifold generator action induced lattice N and its dual-overlattice N^* determining the invariant monomials of this action for example as in [3]. Table 9 show the two pairings together for $n = 0$ where at least a superficial relationship appears to hold. Note that the transitions between $T^*(a)$ and $N^*(\alpha)$ are reminiscent of the level-lowering transitions within endpoint families for levels $n \leq -1$.

$\alpha :$	$T^*(\alpha) :$	$N^*(\alpha) :$	$N^*(T^*(\alpha)) :$	$\alpha :$	$T^*(\alpha) :$	$N^*(\alpha) :$	$N^*(T^*(\alpha)) :$
77	222332222	2222332222 [†]	636 [†]				
76	222332222	2222332222	536 [†]				
75	22332222	222233222	436 [†]				
74	2332222	22223322	336	54	23322	222322	334
73	332222	222232	236	53	3322	22232	234
733	2432222	22223322 [†]	3236 [†]	533	24322	222332	3234 [†]
742	3332222	2222323 [†]	2336 [†]	542	33322	222323	2334 [†]
732	432222	222233	2236	532	4322	22233	2234
7322	532222	222234 [†]	22236	5322	5322	22234	22234
73222	632222	222235 [†]	222236	5	322	2222	24
732222	732222	222236 [†]	222236 [†]	44	2332	22322	333
7	32222	222222	26	43	332	2232	233
66	22233222	22233222	535 [†]	433	2432	22332	3233
65	2233222	22233222	435 [†]	442	3332	22323	2333
64	233222	2223322	335	432	432	2233	2233
63	33222	22232	235	4	32	222	23
633	243222	222332	3235 [†]	33	42	232	223
642	333222	2223323	2335 [†]	333	342	2332	2323
632	43222	22233	2235	3	3	22	22
6322	53222	22234	22235	3333	2442	23332 [†]	32323 [†]
63222	63222	22235	222235	3342	3342	23323 [†]	23323 [†]
6	3222	22222	25				
55	223322	2223222	434 [†]				
\vdots	\vdots	\vdots					

Table 9: T^* versus N^* dual-overlattice pairings for level $n = 0$ endpoints. Entries marked with \dagger are not valid 6D SCFT endpoints.

3.2.1 $n \rightarrow \infty$ endpoint extrapolations

Further indication that T^* and N^* pairing are similar appears upon investigation of the orbifolds defined in the limit $\alpha_{j,\infty} \leftrightarrow k_{u,\infty}/k_{l,\infty}$ by Hirzebruch-Jung continued fraction matching each $\lim_{n \rightarrow \infty} f(n)$. Each gives a valid 6D SCFT endpoint which we collect in Table 13. For example, $\alpha \sim 33$ has αA_n with a large- N limit matching the continued fraction for 23. This set of extrapolated ends is closed under N^* duality. The N^* induced permutation on these 11 symbols is nearly identical to the corresponding T^* duality on the leads $\bar{\alpha}$ with $33 \xrightarrow{T^*} 42$ replaced with a trivial cycle.

$\bar{\alpha} :$	32222	3222	4	33	322	3	5	42	32	6	7	\emptyset
$\alpha A_\infty :$	A_5	A_4	A_2	23	A_3	32	4	2	3	5	6	\emptyset
$N^*(\alpha A_\infty) :$	6	5	3	32	4	23	A_3	2	A_2	A_4	A_5	\emptyset

Table 10: Ends extrapolated from αA_n as $n \rightarrow \infty$ and their overlattice duals.

4 On 6D SCFT endpoint combinatorics

In this section we provide a few observations concerning rules governing the collection of 6D SCFT endpoints with a focus on the paired rational functions $f(n)$ in terms of their integer ingredients and overall structure. We begin by working towards a simple description of the permitted linear 6D SCFT endpoint continued fraction formulas. We find an identity that holds for all linear endpoint linked $f(n)$ sufficient to determine the permitted endpoint families via the handful of allowed fraction determinant values. We extend the same approach to D-type endpoint families.

In addition to the row invariant values detailed in Table 13, there are two other row invariant quantities: the residues of $f(n)$ and $1/f(n)$ at their poles. Surprisingly, the latter precisely match the fraction determinant values as shown in Table 11. The correspondence is more than set-wise. Rather, we have a direct matching which reads

$$[\text{Res}_{n=n_c}(\frac{q}{p}(\alpha A_n \beta))]^{-1} = \sqrt{-\det(\frac{p}{q}(\bar{\beta} A_n \bar{\alpha}))}, \quad (4.1)$$

with each side depending only on β . This identity lets one easily check whether $\det(f(n))$ and $\det(\bar{f}(n))$ both are negated squares of the first six positive integers without first computing both $f(\bar{\gamma}_n)$ and $f(\gamma_n)$. In considering the integer parameters yielding valid $f(n)$, this allows us to determine those cases which have $\det(f(n))$ and $\det(\bar{f}(n))$ both meeting this determinant condition. Upon constraining to those cases obeying 2.6 we find precisely those $f(n)$ in contact with 6D SCFT bases as we discuss shortly in greater detail.

$\bar{\alpha} :$	32222	3222	4	33	322	3	5	42	32	6	7	\emptyset
$[\text{Res}_{n=n_c}(\frac{q}{p}(\alpha A_n \beta))]^{-1} :$	6^2	5^2	3^2	5^2	4^2	2^2	4^2	5^2	3^2	5^2	6^2	1

Table 11: Inverses of residue value for $1/f(n)$ at its pole n_c for $\alpha A_n \beta$. Note the β invariance.

We now consider appropriate n shifts so that

$$f(\gamma_n) = \frac{k_u n + r_u}{k_l n + r_l}, \quad f(\bar{\gamma}_n) = \frac{k_u n + r_u}{\tilde{k}_l n + \tilde{r}_l} \quad (4.2)$$

holds. In most cases, this requires no modification from the minimally shifted expression. Rearranging (4.1) yields

$$\det(f(\gamma_n)) \det(f(\bar{\gamma}_n)) = k_u^2. \quad (4.3)$$

Using (2.6) gives $\gcd(k_u, k_l) \cdot \gcd(k_u, \tilde{k}_l) = k_u$.

This constraint allows for straightforward computation of $f(n)$ from $\bar{f}(n)$ and enables an alternate characterization of 6D SCFT base compatible $f(n)$. This also makes clear that unordered integer pairs $\{\det(f(n)), \text{Res}(f(n))\}$ are preserved by T^* pairing (and endpoint

reversal). We list these pairs explicitly as Table 12 and find that T^* pairs with matching unordered integer pairs appear to be precisely those with fixed N_a size.

$\alpha \backslash \beta$	7	6	5	4	42	3	33	32	322	3222	32222	2
7	{6, 6}	{5, 6}	{4, 6}	{3, 6}	{5, 6}	{2, 6}	{5, 6}	{3, 6}	{4, 6}	{5, 6}	{6, 6}	{1, 6}
6	{6, 5}	{5, 5}	{4, 5}	{3, 5}	{5, 5}	{2, 5}	{5, 5}	{3, 5}	{4, 5}	{5, 5}	{6, 5}	{1, 5}
5	{6, 4}	{5, 4}	{4, 4}	{3, 4}	{5, 4}	{2, 4}	{5, 4}	{3, 4}	{4, 4}	{5, 4}	{6, 4}	{1, 4}
4	{6, 3}	{5, 3}	{4, 3}	{3, 3}	{5, 3}	{2, 3}	{5, 3}	{3, 3}	{4, 3}	{5, 3}	{6, 3}	{1, 3}
24	{6, 5}	{5, 5}	{4, 5}	{3, 5}	{5, 5}	{2, 5}	{5, 5}	{3, 5}	{4, 5}	{5, 5}	{6, 5}	{1, 5}
3	{6, 2}	{5, 2}	{4, 2}	{3, 2}	{5, 2}	{2, 2}	{5, 2}	{3, 2}	{4, 2}	{5, 2}	{6, 2}	{1, 2}
33	{6, 5}	{5, 5}	{4, 5}	{3, 5}	{5, 5}	{2, 5}	{5, 5}	{3, 5}	{4, 5}	{5, 5}	{6, 5}	{1, 5}
23	{6, 3}	{5, 3}	{4, 3}	{3, 3}	{5, 3}	{2, 3}	{5, 3}	{3, 3}	{4, 3}	{5, 3}	{6, 3}	{1, 3}
223	{6, 4}	{5, 4}	{4, 4}	{3, 4}	{5, 4}	{2, 4}	{5, 4}	{3, 4}	{4, 4}	{5, 4}	{6, 4}	{1, 4}
2223	{6, 5}	{5, 5}	{4, 5}	{3, 5}	{5, 5}	{2, 5}	{5, 5}	{3, 5}	{4, 5}	{5, 5}	{6, 5}	{1, 5}
22223	{6, 6}	{5, 6}	{4, 6}	{3, 6}	{5, 6}	{2, 6}	{5, 6}	{3, 6}	{4, 6}	{5, 6}	{6, 6}	{1, 6}
2	{6, 1}	{5, 1}	{4, 1}	{3, 1}	{5, 1}	{2, 1}	{5, 1}	{3, 1}	{4, 1}	{5, 1}	{6, 1}	{1, 1}

Table 12: Pairs $(\sqrt{-\det(f(n))}, \sqrt{-\text{Res}(1/f(n))})$. Note that T^* pairing visible as reflection about the antidiagonal in the upper 11×11 block and the $\alpha \sim 3$ entry in the final column preserves all unordered pairs.

4.1 From relations to SCFT compatible orbifolds

In this section we discuss two characterizations of the rational functions $f(n)$ giving valid 6D SCFT endpoints. The first involves only the integers $1 \leq k \leq 6$ and relations on fraction determinants. The second involves the values which can arise in the limit $\lim_{n \rightarrow \infty} f(n)$. A key ingredient in our setup is that we only consider rational functions of the form (2.4).

In each case, precisely the minimally n shifted endpoint family generators $f(n)$ are obtained by augmenting the constraint (2.4). Our aim is to step towards a parsimonious description of endpoint families short of requiring the Calabi-Yau condition on elliptic fibrations. Consider all $f(n)$ as in (2.4) obeying (2.6) up to orientation of strings m_1, \dots, m_k (as in (2.2)) and equivalence of orbifold families they determine (i.e. by reducing the expressions $f(n)$ under consideration by minimally shifted n).³ Next impose that $\det(f(n)) = -s^2$ for $1 \leq s \leq 6$ an integer. This gives two simple sets of constraints which leave precisely the desired $f(n)$.

Briefly, the following three requirements determine everything:

- $\sqrt{-\det(f(n))} \in \{1, \dots, 6\}$,
- $f(n)$ satisfy (2.6),
- (a): $(\sqrt{\text{Res}(1/f(n))}) = \sqrt{-\det(\bar{f}(n))} \in \{1, \dots, 6\}$ or (b) Large N limits must lie in L_∞ .

³Note that certain orbifold families with $f(n)$ of the form (2.4) are equivalent to others having distinct $f(n)$ by a shift of n . We discard without loss of generality all $f(n)$ having non-minimal non-negative or negative values of r_u, r_l .

4.1.1 The permitted $f(n)$ from $\det(\bar{f}(n))$

One approach is simply to require that $-\det(\bar{f}(n)), -\det(f(n)) \in \{1^2, \dots, 6^2\}$. Note that it is convenient to compute the former as $[\text{Res}_{n=n_c}(\frac{1}{f(n)})]^{-1}$. The trivial requirement that $q \leq p$ (as these determine equivalent orbifolds) in all remaining $f(n)$ can be taken without loss of generality. Explicit enumeration confirms that only precisely those $f(n)$ which correspond to 6D SCFT endpoint families remain.

4.1.2 The permitted $f(n)$ from their large n limits

Alternatively, we can augment the determinant constraints with the minimal data set consisting of the 12 rationals giving permitted large n limits. These k_u/k_l values for $f(\alpha A_n \beta)$ are β invariant (i.e. fixed on rows of Table 1, as are the aforementioned residues) and appear as Table 13. Let us refer to these twelve rationals as L_∞ . Note that these are precisely the rationals $r = a/b \in \mathbb{Q}$ with $1 \leq r, a, b \leq 6$. As an aside, numerators of these row invariants match the corresponding column invariants $\sqrt{-\det(f(n))}$ appearing in Table 3. All $f(n)$ are fully determined by the values in L_∞ with the requirement that $\lim_{n \rightarrow \infty} f(n) \in L_\infty$ as we can confirm by explicit enumeration of the possible matches subject to the first two fraction determinant constraints above. This approach precisely recovers the permitted minimally shifted $f(n)$ that arise from 6D SCFT endpoints.

$\bar{\alpha} :$	32222	3222	4	33	322	3	5	42	32	6	7	\emptyset
$\frac{k_u}{k_l} :$	$\frac{6}{5}$	$\frac{5}{4}$	$\frac{3}{2}$	$\frac{5}{3}$	4	2	$\frac{4}{3}$	$\frac{5}{2}$	3	5	6	1

Table 13: Values of $\frac{k_u}{k_l}(\alpha) = \lim_{n \rightarrow \infty} f(\alpha A_n \beta)$.

4.2 Intermediate determinants and canonical bases

In [2], the intermediate quotient Γ/H was discussed in relation to the truncations of bases for each endpoint string, where H is the kernel of the map $\det : \Gamma \rightarrow U(1)$. In this section we offer a few further comments along these lines. We give the intermediate quotient Γ/H for $H := \ker(\det : \Gamma \rightarrow U(1))$ having order m and k/l giving the generator $e^{2\pi i \cdot \frac{l}{k}}$ of Γ/H . The values $(m, k/l)$ appeared in [2]. Here we display them in terms of n to give the minimally n shifted $f(n)$ and lead ordering evidently respecting T^* pairing.

We compute the values m as $p/(\text{den}(\frac{q+1}{p}))$ where ‘den’ denotes the denominator of a rational written in lowest terms. The values l/k are then simply obtained as $l = \frac{q+1}{m}$ and $k = \frac{p}{m}$. As noted in [2] we have $\frac{p}{q+1} = m \frac{k}{l}$ with k, l relatively prime. We observe that reflection about the antidiagonal in each block diagonal group (with n -coefficient of m given by $d \in \{1, \dots, 6\}$) corresponds to endpoint reversal. Blocks consist precisely those endpoints built as $\alpha A_n \bar{\beta}$ from tails with matching fraction determinant, i.e. $\det(\alpha) = \det(\beta)$.

Minimal resolutions of each endpoint give one distinguished class of bases as discussed in [6] by blowing up as little as possible to obtain a valid F-theory base in each

$\alpha \backslash \beta$	32222	7	6	42	33	3222	5	322	4	32	3	0	
7	$(6(n+1), 6)$	$(2(3n+1), 6)$	$(1, \frac{30n+11}{5n+2})$	$(1, \frac{30n+17}{5n+3})$	$(1, \frac{30n+23}{5n+4})$	$(1, \frac{30n+29}{5n+5})$	$(2, \frac{12n+5}{9n+1})$	$(2, \frac{12n+11}{9n+2})$	$(1, \frac{18n+9}{3n+2})$	$(3, \frac{6n+5}{n+1})$	$(2, \frac{6n+1}{n+1})$	$(1, \frac{6n+1}{n+1})$	
22223	$(2(3n+2), \frac{6}{5})$	$(6(n+1), \frac{6}{5})$	$(1, \frac{30n+11}{25n+1})$	$(1, \frac{30n+17}{25n+6})$	$(1, \frac{30n+23}{25n+11})$	$(1, \frac{30n+29}{25n+16})$	$(2, \frac{12n+11}{10n+1})$	$(2, \frac{12n+17}{10n+6})$	$(3, \frac{6n+1}{5n+1})$	$(1, \frac{18n+9}{5n+8})$	$(2, \frac{6n+2}{5n+2})$	$(1, \frac{6n+5}{5n+5})$	
2223	$(1, \frac{30n+15}{24n+15})$	$(1, \frac{30n+21}{24n+21})$	$(5(n+1), \frac{5}{4})$	$(5n+1, \frac{5}{4})$	$(5n+2, \frac{5}{4})$	$(5n+3, \frac{5}{4})$	$(1, \frac{20n+11}{16n+1})$	$(1, \frac{20n+17}{16n+6})$	$(1, \frac{15n+2}{12n+2})$	$(1, \frac{15n+7}{12n+7})$	$(1, \frac{10n+3}{8n+3})$	$(1, \frac{5n+4}{4n+4})$	
33	$(1, \frac{30n+12}{15n+9})$	$(1, \frac{30n+18}{15n+15})$	$(5n+4, \frac{5}{3})$	$(5(n+1), \frac{5}{3})$	$(5n+1, \frac{5}{2})$	$(5n+2, \frac{5}{2})$	$(1, \frac{20n+11}{8n+7})$	$(1, \frac{20n+17}{8n+12})$	$(1, \frac{15n+2}{6n+6})$	$(1, \frac{15n+7}{6n+11})$	$(1, \frac{10n+1}{4n+4})$	$(1, \frac{5n+3}{2n+2})$	
24	$(1, \frac{30n+17}{18n+14})$	$(1, \frac{30n+23}{18n+20})$	$(5n+3, \frac{5}{3})$	$(5n+4, \frac{5}{3})$	$(5(n+1), \frac{5}{3})$	$(5n+1, \frac{5}{2})$	$(1, \frac{20n+13}{12n+8})$	$(1, \frac{20n+19}{12n+13})$	$(1, \frac{15n+11}{9n+7})$	$(1, \frac{15n+16}{9n+12})$	$(1, \frac{10n+9}{6n+6})$	$(1, \frac{5n+2}{3n+2})$	
6	$(1, \frac{30n+31}{6n+6})$	$(1, \frac{30n+37}{6n+12})$	$(5n+2, 5)$	$(5n+3, 5)$	$(5n+4, 5)$	$(5(n+1), 5)$	$(1, \frac{20n+9}{4n+4})$	$(1, \frac{20n+15}{4n+10})$	$(1, \frac{15n+8}{3n+2})$	$(1, \frac{15n+13}{3n+7})$	$(1, \frac{10n+7}{2n+2})$	$(1, \frac{5n+1}{n+1})$	
223	$(2, \frac{12n+7}{9n+5})$	$(2, \frac{12n+13}{9n+11})$	$(1, \frac{20n+19}{15n+14})$	$(1, \frac{20n+25}{15n+20})$	$(1, \frac{20n+31}{15n+26})$	$(1, \frac{20n+37}{15n+32})$	$(1, \frac{20n+11}{15n+8})$	$(4(n+1), \frac{4}{3})$	$(2(2n+1), \frac{4}{3})$	$(1, \frac{12n+1}{9n+1})$	$(1, \frac{12n+5}{9n+5})$	$(2, \frac{4n+1}{3n+1})$	$(1, \frac{4n+3}{3n+3})$
5	$(2, \frac{12n+13}{3n+3})$	$(2, \frac{12n+19}{3n+9})$	$(1, \frac{20n+9}{5n+2})$	$(1, \frac{20n+15}{5n+8})$	$(1, \frac{20n+21}{5n+14})$	$(1, \frac{20n+27}{5n+20})$	$(1, \frac{20n+11}{5n+5})$	$(2(2n+1), 4)$	$(4(n+1), 4)$	$(1, \frac{12n+7}{3n+2})$	$(1, \frac{12n+11}{3n+7})$	$(2, \frac{4n+3}{n+1})$	$(1, \frac{4n+1}{n+1})$
23	$(1, \frac{18n+9}{12n+5})$	$(3, \frac{6n+5}{4n+3})$	$(1, \frac{15n+13}{10n+8})$	$(1, \frac{15n+19}{10n+14})$	$(1, \frac{15n+25}{10n+20})$	$(1, \frac{15n+31}{10n+26})$	$(1, \frac{15n+7}{10n+4})$	$(1, \frac{12n+11}{8n+7})$	$(1, \frac{12n+15}{8n+11})$	$(3(n+1), \frac{3}{2})$	$(3n+1, \frac{3}{2})$	$(1, \frac{6n+1}{3n+1})$	$(1, \frac{3n+2}{2n+2})$
4	$(3, \frac{6n+7}{2n+2})$	$(1, \frac{18n+9}{6n+2})$	$(1, \frac{15n+8}{5n+2})$	$(1, \frac{15n+14}{5n+8})$	$(1, \frac{15n+20}{5n+14})$	$(1, \frac{15n+26}{5n+20})$	$(1, \frac{15n+17}{5n+11})$	$(1, \frac{12n+17}{4n+2})$	$(1, \frac{12n+23}{4n+8})$	$(3n+2, 3)$	$(3(n+1), 3)$	$(1, \frac{6n+5}{3n+2})$	$(1, \frac{3n+1}{2n+1})$
3	$(2, \frac{6n+8}{3n+3})$	$(2, \frac{6n+14}{3n+9})$	$(1, \frac{10n+7}{5n+2})$	$(1, \frac{10n+13}{5n+8})$	$(1, \frac{10n+19}{5n+14})$	$(1, \frac{10n+25}{5n+20})$	$(1, \frac{10n+13}{5n+5})$	$(2, \frac{4n+3}{2n+1})$	$(2, \frac{4n+9}{2n+7})$	$(1, \frac{6n+5}{3n+2})$	$(1, \frac{6n+11}{3n+8})$	$(2(n+1), 2)$	$(1, \frac{2n+1}{n+1})$
0	$(1, \frac{6n+11}{6n+6})$	$(1, \frac{6n+17}{6n+12})$	$(1, \frac{6n+6}{6n+2})$	$(1, \frac{6n+12}{6n+8})$	$(1, \frac{6n+18}{6n+14})$	$(1, \frac{6n+24}{6n+20})$	$(1, \frac{6n+9}{6n+5})$	$(1, \frac{6n+15}{6n+11})$	$(1, \frac{6n+7}{4n+1})$	$(1, \frac{6n+13}{4n+7})$	$(1, \frac{6n+5}{3n+3})$	$(1, \frac{6n+1}{2n+1})$	$(n+1, 1)$

Table 14: Values of $(m, k/l)$ giving the order of $H := \ker(\det : \Gamma \rightarrow U(1))$ and generator $e^{2\pi i \frac{l}{k}}$ of the intermediate group Γ/H . Note that the block groupings respect the T^* pairing expressed as transposition of the grid.

$d \backslash \gamma$	
6	$2231513221(\overbrace{\{12\}12231513221}^{n+1}) \cdots \{12\}1223151322$
5	$231513221(\overbrace{\{12\}12231513221}^{n+1}) \cdots \{12\}122315132$
4	$2321(\overbrace{812321}^{n+1}) \cdots 81232$
3	$31(\overbrace{6131}^{n+1}) \cdots 613$
2	$(\overbrace{41}^{n+1}) \cdots 4$
1	$(\overbrace{2}^{n+1}) \cdots 0$

Table 15: Level n bases γ yielding block diagonal endpoint groups with common $\det : \Gamma \rightarrow U(1)$ behavior with n coefficient of m given by d . The terms in parentheses are repeated $n+1$ times.

endpoint. One sided truncations of the possible minimal resolutions are known to comprise the available block diagonal endpoint groupings of the intermediate determinant map $\det : \Gamma \rightarrow U(1)$ as discussed in [2] and summarized in Table 15. However, the remaining endpoints require moving slightly beyond minimal resolution to give a similar characterization. (Consolidating instantons after blowing up slightly past a minimal resolution makes the relationship between common determinant behavior groups and truncation behavior of resolutions evident as a generalization of Table 15.)

The collection of near minimal resolutions is structurally somewhat unwieldy in comparison with a certain class of linear endpoint base representatives we will term *canonical endpoint representatives* or *canonical bases* obtained as the truncations of a single (infinite) chain of curves. As recently reported in [8], these biject with linear endpoints to cleanly

characterize the 12×12 endpoint family structure as left and right truncations of the bases

$$\overbrace{12231513221}^{L_l} \overbrace{(\langle 12 \rangle 12231513221) \cdots \langle 12 \rangle}^n \overbrace{12231513221}^{L_r} . \quad (4.4)$$

This structure induces a unique canonical ordering of leads/tails that T^* pairing respects as does the common intermediate determinant behavior in each block diagonal group as is evident in Table 14. Rows and columns correspond to one sided truncations of a fixed canonical base, transposition to endpoint reversal, and T^* pairing to reflection about the 11×11 block antidiagonal.

Inclusion induced structure endows each level- n endpoint set with a unique canonical partial order compatible with the truncation induced lead ordering and T^* compatible symmetric lead ordering. The left/right truncations of L_l, L_r in the fixed- n base in (4.4) yields the level n endpoints by blowing down with an n -shift obtained by replacing the empty lead by a single -2 curve. This places a natural level relation between endpoint families (i.e. a natural family-wise fixed choice of shift $n \rightarrow \tilde{n}$ for each). The inclusion structure places a partial ordering on endpoints in each level compatible with the strict ordering on leads

$$H = \{7, 6, 5, 4, 24, 3, 33, 23, 223, 2223, 22223, 2\} , \quad (4.5)$$

in order corresponding to increasingly truncated strings from (4.4).

This truncation induced lead order is compatible with the symmetric T^* induced orderings where all integral p -roots lie on the 11×11 anti-diagonal. This ordering hence singles out a unique T^* compatible lead ordering. The resulting signs of p roots modulo 1 notably appearing in large blocked groups which we display with the induced n shift and ordering in Table 2.

A further relationship holds between T^* paired endpoints and the structure of bases $b_{l,r,n}$ with form (4.4). The T^* paired bases $b_{i,j,n}, b_{i,j,n}^*$ have the following two properties.

- The combined total number of curves in each pair is constant for fixed n .
- The paired bases permit a gluing by introducing a single curve.

Each follows from the relationship of T^* pairing with endpoint/canonical base pairing. Together these make clear that T^* pairing respects a simple truncation structure with each T^* pair naturally associated to a unique longer base and hence (distinct) endpoint.

Regularity in the structure of linear 6D SCFT endpoint families is revealed by the above truncation structure. A graph can be defined on endpoint families by joining those that contain bases of the form (4.4) which are minimally truncation related, i.e. differing by a single curve. This graph Γ_e is illustrated in Figure 2. It has automorphism group $G \cong D_{12}$ of order 24 with orbits of sizes $12^6, 6$ (and generators acting by (i) separately cycling the 6 central points and the radial bands of shared lead simultaneously and (ii,iii) reflection about an opposite pair of outermost vertices where for (ii) these are 4-valent and leave 8 fixed points while for (iii) these are 2-valent and leave 6 fixed points). The order

two generator g_a of type (ii) above corresponds to T^* pairing (this being the reflection about the line from $v_{1,a} \sim 3A_n3$ to $v_{1,a} \sim \emptyset A_n \emptyset$). The type (iii) generator g_b arises as the reflection about the line between $v_{1,b} \sim 223A_n3222$ and $v_{2,b} \sim 5A_n4$. Note that a less symmetric graph having automorphism group of order 2 results unless we consider multiple levels in this construction.

Forms of $f(n)$ and $\det : \Gamma \rightarrow U(1)$ invariants with this induced lead ordering appear in Table, 16,17, respectively. Note that the T^* pairing respects the n coefficients appearing in m, k .

$\alpha \backslash \beta$	7	6	5	4	42	3	33	32	322	3222	32222	2
7	$\frac{36n+48}{6n+7}$	$\frac{30n+41}{5n+6}$	$\frac{24n+34}{4n+5}$	$\frac{18n+27}{3n+4}$	$\frac{30n+47}{5n+7}$	$\frac{12n+20}{2n+3}$	$\frac{30n+53}{5n+8}$	$\frac{18n+33}{3n+5}$	$\frac{24n+46}{4n+7}$	$\frac{30n+59}{5n+9}$	$\frac{36n+72}{6n+11}$	$\frac{6n+13}{n+2}$
6	$\frac{30n+41}{6n+7}$	$\frac{25n+35}{5n+6}$	$\frac{20n+29}{4n+5}$	$\frac{15n+23}{3n+4}$	$\frac{25n+40}{5n+7}$	$\frac{10n+17}{2n+3}$	$\frac{25n+45}{5n+8}$	$\frac{15n+28}{3n+5}$	$\frac{20n+39}{4n+7}$	$\frac{25n+50}{5n+9}$	$\frac{30n+61}{6n+11}$	$\frac{5n+11}{n+2}$
5	$\frac{24n+34}{6n+7}$	$\frac{20n+29}{5n+6}$	$\frac{16n+24}{4n+5}$	$\frac{12n+19}{3n+4}$	$\frac{20n+33}{5n+7}$	$\frac{8n+14}{2n+3}$	$\frac{20n+37}{5n+8}$	$\frac{12n+23}{3n+5}$	$\frac{16n+32}{4n+7}$	$\frac{20n+41}{5n+9}$	$\frac{24n+50}{6n+11}$	$\frac{4n+9}{n+2}$
4	$\frac{18n+27}{6n+7}$	$\frac{15n+23}{5n+6}$	$\frac{12n+19}{4n+5}$	$\frac{9n+15}{3n+4}$	$\frac{15n+26}{5n+7}$	$\frac{6n+11}{2n+3}$	$\frac{15n+29}{5n+8}$	$\frac{9n+18}{3n+5}$	$\frac{12n+25}{4n+7}$	$\frac{15n+32}{5n+9}$	$\frac{18n+39}{6n+11}$	$\frac{3n+7}{n+2}$
24	$\frac{30n+47}{18n+27}$	$\frac{25n+40}{15n+23}$	$\frac{20n+33}{12n+19}$	$\frac{15n+26}{9n+15}$	$\frac{25n+45}{15n+26}$	$\frac{10n+19}{6n+11}$	$\frac{25n+50}{15n+29}$	$\frac{15n+31}{9n+18}$	$\frac{20n+43}{12n+25}$	$\frac{25n+55}{15n+32}$	$\frac{30n+67}{18n+39}$	$\frac{5n+12}{3n+7}$
3	$\frac{12n+20}{6n+7}$	$\frac{10n+17}{5n+6}$	$\frac{8n+14}{4n+5}$	$\frac{6n+11}{3n+4}$	$\frac{10n+19}{5n+7}$	$\frac{4n+8}{2n+3}$	$\frac{10n+21}{5n+8}$	$\frac{6n+13}{3n+5}$	$\frac{8n+18}{4n+7}$	$\frac{10n+23}{5n+9}$	$\frac{12n+28}{6n+11}$	$\frac{2n+5}{n+2}$
33	$\frac{30n+53}{12n+20}$	$\frac{25n+45}{10n+17}$	$\frac{20n+37}{8n+14}$	$\frac{15n+29}{6n+11}$	$\frac{25n+50}{10n+19}$	$\frac{10n+21}{4n+8}$	$\frac{25n+55}{10n+21}$	$\frac{15n+34}{6n+13}$	$\frac{20n+47}{8n+18}$	$\frac{25n+60}{10n+23}$	$\frac{30n+73}{12n+28}$	$\frac{5n+13}{2n+5}$
23	$\frac{18n+33}{12n+20}$	$\frac{15n+28}{10n+17}$	$\frac{12n+23}{8n+14}$	$\frac{9n+18}{6n+11}$	$\frac{15n+31}{10n+19}$	$\frac{6n+13}{4n+8}$	$\frac{15n+34}{10n+21}$	$\frac{9n+21}{6n+13}$	$\frac{12n+29}{8n+18}$	$\frac{15n+37}{10n+23}$	$\frac{18n+45}{12n+28}$	$\frac{3n+8}{2n+5}$
223	$\frac{24n+46}{18n+33}$	$\frac{20n+39}{15n+28}$	$\frac{16n+32}{12n+23}$	$\frac{12n+25}{9n+18}$	$\frac{20n+43}{15n+31}$	$\frac{8n+18}{6n+13}$	$\frac{20n+47}{15n+34}$	$\frac{12n+29}{9n+21}$	$\frac{16n+40}{12n+29}$	$\frac{20n+51}{15n+37}$	$\frac{24n+62}{18n+45}$	$\frac{4n+11}{3n+8}$
2223	$\frac{30n+59}{24n+46}$	$\frac{25n+50}{20n+39}$	$\frac{20n+41}{16n+32}$	$\frac{15n+32}{12n+25}$	$\frac{25n+55}{20n+43}$	$\frac{10n+23}{8n+18}$	$\frac{25n+60}{20n+47}$	$\frac{15n+37}{12n+29}$	$\frac{20n+51}{16n+40}$	$\frac{25n+65}{20n+51}$	$\frac{30n+79}{24n+62}$	$\frac{5n+14}{4n+11}$
22223	$\frac{36n+72}{30n+59}$	$\frac{30n+61}{25n+50}$	$\frac{24n+50}{20n+41}$	$\frac{18n+39}{15n+32}$	$\frac{30n+67}{25n+55}$	$\frac{12n+28}{10n+23}$	$\frac{30n+73}{25n+60}$	$\frac{18n+45}{15n+37}$	$\frac{24n+62}{20n+51}$	$\frac{30n+79}{25n+65}$	$\frac{36n+96}{30n+79}$	$\frac{6n+17}{5n+14}$
2	$\frac{6n+13}{6n+7}$	$\frac{5n+11}{5n+6}$	$\frac{4n+9}{4n+5}$	$\frac{3n+7}{3n+4}$	$\frac{5n+12}{5n+7}$	$\frac{2n+5}{2n+3}$	$\frac{5n+13}{5n+8}$	$\frac{3n+8}{3n+5}$	$\frac{4n+11}{4n+7}$	$\frac{5n+14}{5n+9}$	$\frac{6n+17}{6n+11}$	$\frac{n+2}{n+1}$

Table 16: Truncation compatible ordering and n -shift of $\frac{p}{q}(\alpha A_n \beta)$.

$\alpha \backslash \beta$	7	6	5	4	24	3	33	23	223	2223	22223	2
7	$(2(3n+4), 6)$	$(1, \frac{30n+41}{5n+7})$	$(2, \frac{12n+17}{2n+3})$	$(1, \frac{18n+27}{3n+5})$	$(1, \frac{30n+47}{5n+8})$	$(2, \frac{6n+10}{n+2})$	$(1, \frac{30n+53}{5n+9})$	$(3, \frac{6n+11}{n+2})$	$(2, \frac{12n+23}{2n+4})$	$(1, \frac{30n+59}{5n+10})$	$(6(n+2), 6)$	$(1, \frac{6n+13}{n+3})$
6	$(1, \frac{30n+41}{6n+8})$	$(5n+7, 5)$	$(1, \frac{20n+29}{4n+6})$	$(1, \frac{15n+23}{3n+5})$	$(5n+8, 5)$	$(1, \frac{10n+17}{2n+4})$	$(5n+9, 5)$	$(1, \frac{15n+28}{3n+6})$	$(1, \frac{20n+39}{4n+8})$	$(5(n+2), 5)$	$(1, \frac{30n+61}{6n+12})$	$(1, \frac{5n+11}{n+3})$
5	$(2, \frac{12n+17}{3n+4})$	$(1, \frac{20n+29}{5n+7})$	$(2(2n+3), 4)$	$(1, \frac{12n+19}{3n+5})$	$(1, \frac{20n+33}{5n+8})$	$(2, \frac{4n+7}{n+2})$	$(1, \frac{20n+37}{5n+9})$	$(1, \frac{12n+23}{3n+6})$	$(4(n+2), 4)$	$(1, \frac{20n+41}{5n+10})$	$(2, \frac{12n+25}{3n+6})$	$(1, \frac{4n+9}{n+3})$
4	$(1, \frac{18n+27}{6n+8})$	$(1, \frac{15n+23}{5n+7})$	$(1, \frac{12n+19}{4n+6})$	$(3n+5, 3)$	$(1, \frac{15n+26}{5n+8})$	$(1, \frac{6n+11}{2n+4})$	$(1, \frac{15n+29}{5n+9})$	$(3(n+2), 3)$	$(1, \frac{12n+25}{4n+8})$	$(1, \frac{15n+32}{5n+10})$	$(3, \frac{6n+13}{2n+4})$	$(1, \frac{3n+7}{n+3})$
3	$(1, \frac{30n+47}{18n+28})$	$(5n+8, \frac{5}{2})$	$(1, \frac{20n+33}{12n+20})$	$(1, \frac{15n+26}{9n+16})$	$(5n+9, \frac{5}{2})$	$(1, \frac{10n+19}{6n+12})$	$(5(n+2), \frac{5}{2})$	$(1, \frac{15n+31}{9n+19})$	$(1, \frac{20n+43}{12n+26})$	$(5n+11, \frac{5}{2})$	$(1, \frac{30n+67}{18n+40})$	$(1, \frac{5n+12}{2n+6})$
24	$(2, \frac{6n+10}{3n+4})$	$(1, \frac{10n+17}{5n+7})$	$(2, \frac{4n+7}{2n+3})$	$(1, \frac{6n+11}{3n+5})$	$(1, \frac{10n+19}{5n+8})$	$(2(n+2), 2)$	$(1, \frac{10n+21}{5n+9})$	$(1, \frac{6n+13}{3n+6})$	$(2, \frac{4n+9}{2n+4})$	$(1, \frac{10n+23}{5n+10})$	$(2, \frac{6n+11}{3n+6})$	$(1, \frac{2n+5}{n+3})$
33	$(1, \frac{30n+53}{12n+21})$	$(5n+9, \frac{5}{2})$	$(1, \frac{20n+37}{8n+15})$	$(1, \frac{15n+29}{6n+12})$	$(5(n+2), \frac{5}{2})$	$(1, \frac{10n+21}{4n+9})$	$(5n+11, \frac{5}{2})$	$(1, \frac{15n+34}{6n+14})$	$(1, \frac{20n+47}{8n+19})$	$(5n+12, \frac{5}{2})$	$(1, \frac{30n+73}{12n+29})$	$(1, \frac{5n+13}{2n+6})$
23	$(3, \frac{6n+11}{10n+18})$	$(1, \frac{15n+28}{10n+18})$	$(1, \frac{12n+23}{8n+15})$	$(3(n+2), \frac{3}{2})$	$(1, \frac{15n+31}{10n+20})$	$(1, \frac{6n+13}{4n+9})$	$(1, \frac{15n+34}{10n+22})$	$(3n+7, \frac{3}{2})$	$(1, \frac{12n+29}{8n+19})$	$(1, \frac{15n+37}{10n+24})$	$(1, \frac{18n+45}{12n+29})$	$(1, \frac{3n+8}{2n+6})$
223	$(2, \frac{12n+23}{9n+17})$	$(1, \frac{20n+39}{15n+29})$	$(4(n+2), \frac{4}{3})$	$(1, \frac{12n+25}{9n+19})$	$(1, \frac{20n+43}{15n+32})$	$(2, \frac{4n+9}{3n+7})$	$(1, \frac{20n+47}{15n+35})$	$(1, \frac{12n+29}{9n+22})$	$(2(2n+5), \frac{4}{3})$	$(1, \frac{20n+51}{15n+38})$	$(2, \frac{12n+25}{9n+23})$	$(1, \frac{4n+11}{5n+9})$
2223	$(1, \frac{30n+59}{24n+47})$	$(5(n+2), \frac{5}{2})$	$(1, \frac{20n+41}{16n+33})$	$(1, \frac{15n+32}{12n+26})$	$(5n+11, \frac{5}{2})$	$(1, \frac{10n+23}{4n+10})$	$(5n+12, \frac{5}{2})$	$(1, \frac{15n+37}{8n+19})$	$(1, \frac{20n+51}{16n+41})$	$(5n+13, \frac{5}{2})$	$(1, \frac{30n+79}{24n+63})$	$(1, \frac{5n+14}{4n+12})$
22223	$(6(n+2), \frac{6}{5})$	$(1, \frac{30n+61}{25n+51})$	$(2, \frac{12n+25}{10n+21})$	$(3, \frac{6n+13}{5n+11})$	$(1, \frac{30n+67}{25n+56})$	$(2, \frac{6n+10}{5n+12})$	$(1, \frac{30n+73}{25n+61})$	$(1, \frac{18n+45}{15n+38})$	$(2, \frac{12n+26}{10n+26})$	$(1, \frac{30n+79}{25n+66})$	$(2(3n+8), \frac{6}{5})$	$(1, \frac{6n+17}{5n+15})$
2	$(1, \frac{6n+13}{6n+8})$	$(1, \frac{5n+11}{5n+7})$	$(1, \frac{4n+9}{4n+6})$	$(1, \frac{3n+7}{3n+5})$	$(1, \frac{5n+12}{5n+8})$	$(1, \frac{2n+5}{2n+4})$	$(1, \frac{5n+13}{5n+9})$	$(1, \frac{3n+8}{3n+6})$	$(1, \frac{4n+11}{4n+8})$	$(1, \frac{5n+14}{5n+10})$	$(1, \frac{6n+17}{6n+12})$	$(n+2, 1)$

Table 17: Truncation induced ordering and n -shifted values of $(m, k/l)$ describing $\det : \Gamma \rightarrow U(1)$.

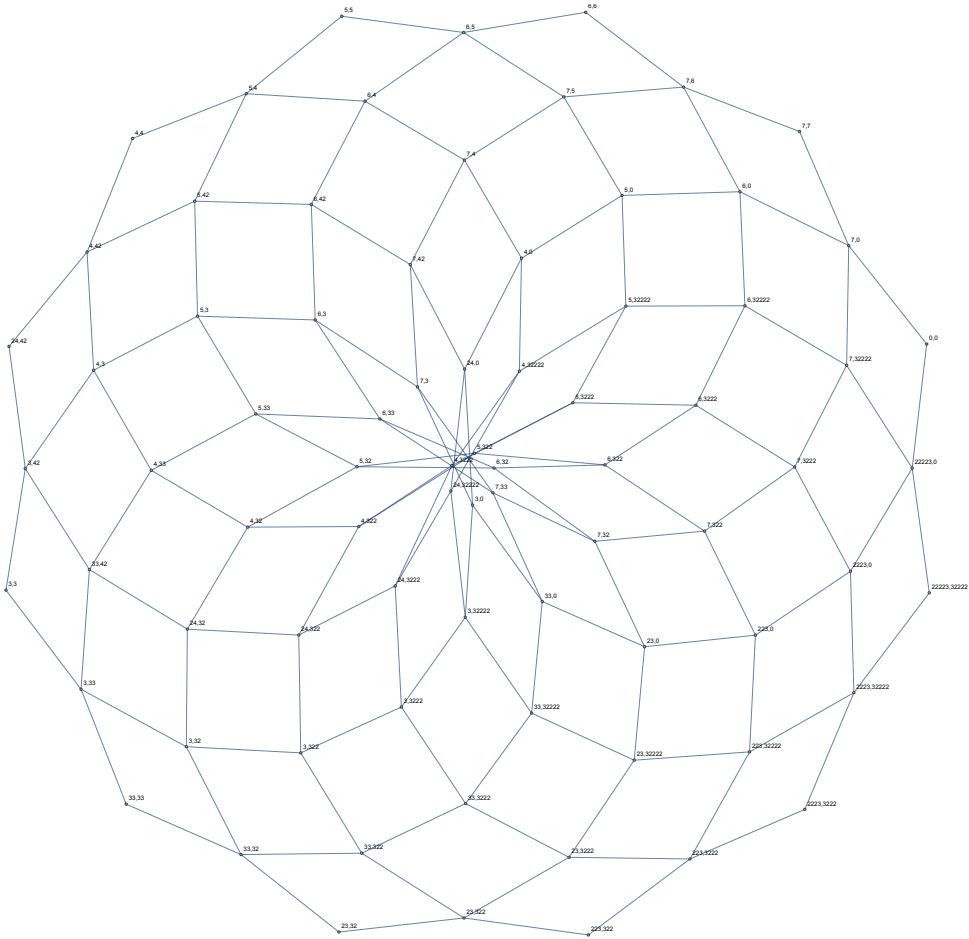


Figure 2: Linear 6D SCFT endpoint families with edges joining nearest truncation of canonical base representatives with form (4.4).

We can similarly define truncation induced graphs from the collection of endpoints which blow down from truncations of L_l, L_r in

$$b_{l,r,n} \sim \overbrace{12321}^{L_l} \overbrace{(\langle 8 \rangle 12321) \cdots (\langle 8 \rangle)}^n \overbrace{12321}^{L_r}. \quad (4.6)$$

This analogously yields a smaller graph with automorphism group $G \cong D_6$ again with one of the order two generators corresponding to T^* pairing.

4.3 SCFT endpoint families and $PSL(2, p)$

Group homomorphisms $\Gamma \subset U(2) \rightarrow E_8 \times E_8$ pairing with 6D SCFTs having an F-theory realization (e.g. $f_{i,j}(n) \leftrightarrow \Gamma$) arise naturally and have been studied at length [6, 8]. All of the well-understood and already classified homomorphisms into $E_8 \times E_8$ from ADE subgroups of $SU(2)$ can be achieved in this way. The discrete $U(2)$ gauge fields of 6D SCFTs do

not however exhaust the list of all finite $U(2)$ subgroups. Current characterizations of the collection $U(2)$ subgroups that pair with 6D SCFTs have yet to match it to any known combinatorial structure in the mathematics literature. While we will not remedy this situation here, it motivates us to outline the following (distinct) way in which entire SCFT endpoint families give rise to group homomorphisms from cyclic groups into $E_8 \times E_8$.

This approach arises as a consequence of the $\det(f(n))$ behavior we have seen which allows the permitted $f(n)$ to be viewed as linear fractional transformations over certain finite fields. Each endpoint family pairs with such a matching rational function upon the replacement $n \mapsto -n$ that reverses level indexing. The resulting permitted values of $\det(f(n))$ are generally squares modulo p (and exhausting the squares in $\mathbb{F}_{p \leq 13}$). We can reduce these rational functions modulo p to give a subset of $G = PSL(2, p)$ for various primes $p \geq 7$ (which generates G for $7 \leq p < 241$ and some larger p). Only for symmetric endpoints is the result independent of endpoint reversal (e.g. $3A_n 32$ versus $23A_n 3$), but we can map from $PSL(2, p) \times PSL(2, p)$ with a natural ordering of summands across all endpoint families induced by canonical base truncation.

We will not fully explore this collection of maps here but wish to note these maps (somewhat trivially) factor through certain simple groups for some p . For example, via Carmichael's constructions [9] of the Steiner systems $S(5, 6, 12)$ and $S(5, 8, 24)$ with automorphism groups M_{12}, M_{24} , we see that each $f(n)$ can be viewed in each group by its action on blocks. (Recall, this approach involves letting linear fractional transformations act on the blocks, for example with $S(5, 6, 12)$ the block of squares in P_{11}

$$B \sim \{\infty, 1, 3, 4, 5, 9\} \tag{4.7}$$

gives under these actions

$$z \mapsto f(z) = \frac{az + b}{cz + d} \quad \text{such that} \quad a, b, c, d \in P_{11}, \quad \det(f(z)) = \overline{s^2} \in P_{11} \tag{4.8}$$

the blocks of $S(5, 6, 12)$.) In other words, we can view each oriented SCFT endpoint family as an element (or its generated cycle) in $PSL(2, 11)$ and consequently also as an element in M_{11} . Similarly reducing modulo 23 leads to elements in $PSL(2, 23)$ and embeddings into M_{24} via action instead on

$$B \sim \{\infty, 0, 1, 3, 12, 15, 21, 22\} \tag{4.9}$$

as a block with elements in P_{23} . These extend to various embeddings into $E_8 \times E_8$ for certain $p \leq 61$ via the classification [10] of simple group homomorphisms into E_8 .

5 Conclusions

We have detailed several structural features of the landscape of 6D SCFTs having an F-theory description including a simple description of the rational functions $f(n)$ that define their endpoint families. Among these is a novel T^* pairing of endpoint families which typically yields precisely matching gauge algebra structures for the theories in paired

families at sufficient level in the tower of 6D SCFT endpoints. We have confined our discussion primarily to linear bases and endpoints for computational ease, perhaps at the expense of a more precise matching to be sought in future work also including branching bases and endpoints. We hope that the pairing detailed here may help via study of T^* paired gauge algebra structure to provide checks on the classification of 6D SCFTs.

Acknowledgments

We would like to thank David R. Morrison and Marco Bertolini for valuable discussions. We are grateful to The UCSB Department of Mathematics for hospitality during the course of this work.

A Expression of discrete $U(2)$ subgroup generators from leads/tails

We pause to review a condensed description of the fraction formulas in Table 1 taken from [11]. This identity illustrates that certain patterns appear among $f(n)$ that are related to lead/tail continued fractions but also depend critically on their matrix representations. This makes clear why certain superficial patterns are broken in some cases, namely those where nontrivial terms in these matrix representations come into play.

It will be convenient to first collect values for the continued fractions for leads/tails. These appear in Table 18. For convenience, we write p_α, q_α in place of $p(\alpha), q(\alpha)$, respectively, except for the empty lead $\alpha \sim \emptyset$ where we write $p_\alpha = 0$. First column entries of

$\alpha :$	\emptyset	3	4	5	6	7	33	23	32	223	322	2223	3222	22223	32222	24	42
$\frac{p_\alpha}{q_\alpha} :$	0	3	4	5	6	7	$\frac{8}{3}$	$\frac{5}{3}$	$\frac{5}{2}$	$\frac{7}{5}$	$\frac{7}{3}$	$\frac{9}{7}$	$\frac{9}{4}$	$\frac{11}{9}$	$\frac{11}{5}$	$\frac{7}{4}$	$\frac{7}{2}$

Table 18: Continued fraction values for lead endpoints.

the Hirzebruch-Jung continued fraction matrix representation [3] for the leading string, α , play a key role. Negations of these values in Table 19 which we label as $m_{\alpha,1}, m_{\alpha,2}$. The

$\alpha :$	3,4,5,6,7	23	223	2223	22223	33	24
$(m_{\alpha,1} \ m_{\alpha,2}) :$	(0 1)	(1 2)	(2 3)	(3 4)	(4 5)	(1 3)	(1 2)

Table 19: First column entries of the Hirzebruch-Jung continued fraction matrix representation for endpoint strings.

78 permitted 6D SCFT paired $f(n)$ giving all orbifold isomorphism classes for endpoints of the form $\alpha A_n \beta$ with $\alpha, \beta \in H$ can then be expressed as

$$\frac{p}{q}(\alpha A_n \beta) = \frac{|(p_{\bar{\alpha}} - q_{\bar{\alpha}})(p_\beta - q_\beta)| \cdot n + |\max\{p_\alpha, 1\} \max\{p_\beta, 1\} - q_\beta m_{\alpha,2}(1 - \delta_{\beta,\emptyset})|}{|(q_\alpha - m_{\alpha,1})(p_\beta - q_\beta)| \cdot n + |q_\alpha \max\{p_\beta, 1\} - q_\beta m_{\alpha,1}(1 - \delta_{\beta,\emptyset})|}. \quad (\text{A.1})$$

The absolute values, $\max(-)$, and Kronecker symbol are included so that we may simultaneously treat the cases with empty strings α, β and may otherwise be ignored. Absolute values are in some cases only included to emphasize that these $f(n)$ contain only nonnegative integer coefficients.

B Miscellaneous tables, D-type endpoints

Miscellaneous tables with content peripheral to our discussion appear in this section including p -roots before reduction modulo 1 (Table 21). Details of these patterns are discussed along with the extent to which they constrain permitted fractions in Section 4. In this section we also extend our earlier discussion of fraction formulas to D-type cases.

$\alpha \backslash \beta$	3222	33	42	6	322	5	4	32222	3	32	\emptyset
	$6A_m 7$ \Downarrow	$24A_m 7$ \Downarrow	$33A_m 7$ \Downarrow	$2223A_m 7$ \Downarrow	$5A_m 7$ \Downarrow	$223A_m 7$ \Downarrow	$23A_m 7$ \Downarrow	$7A_m 7$ \Downarrow	$3A_m 7$ \Downarrow	$4A_m 7$ \Downarrow	$\emptyset A_m 7$ \Downarrow
22223	$22223A_n 3222$	$22223A_n 33$	$22223A_n 42$	$22223A_n 6$	$22223A_n 322$	$22223A_n 5$	$22223A_n 4$	$22223A_n 32222$	$22223A_n 3$	$22223A_n 32$	$22223A_n \emptyset$
6	\dagger	$24A_m 3222$ \Downarrow $6A_n 33$	$33A_m 3222$ \Downarrow $6A_n 42$	$2223A_m 3222$ \Downarrow $6A_n 6$	$5A_m 3222$ \Downarrow $6A_n 322$	$223A_m 3222$ \Downarrow $6A_n 5$	$23A_m 3222$ \Downarrow $6A_n 4$	*	$3A_m 3222$ \Downarrow $6A_n 3$	$4A_m 3222$ \Downarrow $6A_n 32$	$\emptyset A_m 3222^\ddagger$ \Downarrow $6A_n \emptyset^\nabla$
24	**	\dagger	$33A_m 33$ \Downarrow $24A_n 42$	*	$5A_m 33$ \Downarrow $24A_n 322$	$223A_m 33$ \Downarrow $24A_n 5$	$23A_m 33$ \Downarrow $24A_n 4$	*	$3A_m 33$ \Downarrow $24A_n 3$	$4A_m 33$ \Downarrow $24A_n 32$	$\emptyset A_m 33^\ddagger$ \Downarrow $24A_n \emptyset^\nabla$
5	**	**	*	*	\dagger	$223A_m 322$ \Downarrow $5A_n 5$	$23A_m 322$ \Downarrow $5A_n 4$	*	$3A_m 322$ \Downarrow $5A_n 3$	$4A_m 322$ \Downarrow $5A_n 32$	$\emptyset A_m 322^\ddagger$ \Downarrow $5A_n \emptyset^\ddagger$
23	*	**	*	*	**	*	\dagger	*	$3A_m 4$ \Downarrow $23A_n 3$	$4A_m 4$ \Downarrow $23A_n 32$	$\emptyset A_m 4^\ddagger$ \Downarrow $23A_n \emptyset^\ddagger$
Self-dual endpoint families											
	$22223A_n 7$	$2223A_n 6$	$223A_n 5$	$23A_n 4$	$3A_n 3^\ddagger$	$3A_n \emptyset^\ddagger$	$\emptyset A_n \emptyset^\ddagger$	$24A_n 33$			

Table 20: Endpoint family pairings. Those families corresponding to * and ** entries appear elsewhere in the table in lower and upper positions, respectively. Those indicated with ‘ \dagger ’ are self-dual. The \ddagger and ∇ symbols indicate infinitely many permitted gauge enhancements for $n = 0$, and $n = -1$ or $n = -2$, respectively.

B.0.1 D-type rational functions $f(n)$.

In place of (2.6), the D-type endpoint family rational functions obey

$$-2 \det(f(n)) = \gcd(k_u, k_l)^2 . \quad (\text{B.1})$$

Note the additional factor of 2 versus (2.6). After minimal n -shift from the forms dating to [1], these appear as

$$\begin{aligned} D_{\tilde{n}}24 &\leftrightarrow \frac{18n+6}{6n+1}, & D_{\tilde{n}}32 &\leftrightarrow \frac{18n+3}{12n+1}, \\ D_{\tilde{n}}23 &\leftrightarrow \frac{8n+4}{4n+1}, & D_{\tilde{n}}22 &\leftrightarrow \frac{2n+2}{2n+1}, \end{aligned} \tag{B.2}$$

where \tilde{n} is an n -shift D_N is the arrangement of -2 curves while $D_N\alpha$ for $\alpha = x_1 \cdots x_n$ denotes

$$\underbrace{2^2 2^2 \cdots 2^2}_{N-2} \alpha. \tag{B.3}$$

One can readily confirm that D-type endpoints are related to their defining $f(n)$ forms in a manner consistent with the row expressions of fixed k_u/k_l for other endpoints.

Recall from [1] the Hirzebruch-Jung continued fraction for D-type Γ generator can be obtained from the pairing

$$2 \overset{2}{y} m_1 m_2 \cdots m_l \leftrightarrow m_l \cdots m_2 m_1 (2y-2) m_1 m_2 \cdots m_l, \tag{B.4}$$

which yields the expressions in (B.2) up to n -shift via

$$\begin{aligned} D_{\tilde{n}}24 &\leftrightarrow 4A_{2n+1}4, & D_{\tilde{n}}32 &\leftrightarrow 23A_{2n+1}32, \\ D_{\tilde{n}}23 &\leftrightarrow 3A_{2n+1}3, & D_{\tilde{n}}22 &\leftrightarrow A_{2n+1}. \end{aligned} \tag{B.5}$$

These are hence manifestly endpoint-orientation independent. We can naturally place entries from (B.2) in a new column of our $f(n)$ table based upon their k_u/k_l ratios.

For linear endpoints it is sufficient to determine the permitted fraction formulas using (2.6) and fixing allowed large N limit values. The same does not hold for D-types where these constraints leave 11 rather than 4 permitted $f(n)$. The extra cases include $f(n)$ arising from $\alpha A_{2n} \beta$ having designated (k_u, k_l) . More generally, positive integer rescaling the left hand side of (2.6) and restricting (k_u, k_l) to valid large N limits simply yields $f(n)$ corresponding to subfamilies of endpoints expressed elsewhere in the table. Cases corresponding to D-types are simply those having an additional interpretation when a second generator acting by $(z_1, z_2) \mapsto (z_2, -z_1)$ yields non-isomorphic orbifolds. In this sense, these p/q values are captured already by the determinant characterization above but a secondary structure gives them further meaning. Note that there are three exceptional ($\epsilon_6, \epsilon_7, \epsilon_8$) branching endpoints which have not been treated in our discussion.

$\alpha \backslash \beta$	7	3222	33	42	6	322	5	4	32222	3	32	\emptyset
22223	2	$\frac{79}{30}$	$\frac{73}{30}$	$\frac{67}{30}$	$\frac{61}{30}$	$\frac{31}{12}$	$\frac{25}{12}$	$\frac{13}{6}$	$\frac{8}{3}$	$\frac{7}{3}$	$\frac{5}{2}$	$\frac{11}{6}$
6	$\frac{41}{30}$	2	$\frac{9}{5}$	$\frac{8}{5}$	$\frac{7}{5}$	$\frac{39}{20}$	$\frac{29}{20}$	$\frac{23}{15}$	$\frac{61}{30}$	$\frac{17}{10}$	$\frac{28}{15}$	$\frac{6}{5}$
24	$\frac{47}{30}$	$\frac{11}{5}$	2	$\frac{9}{5}$	$\frac{8}{5}$	$\frac{43}{20}$	$\frac{33}{20}$	$\frac{26}{15}$	$\frac{67}{30}$	$\frac{19}{10}$	$\frac{31}{15}$	$\frac{7}{5}$
33	$\frac{53}{30}$	$\frac{12}{5}$	$\frac{11}{5}$	2	$\frac{9}{5}$	$\frac{47}{20}$	$\frac{37}{20}$	$\frac{29}{15}$	$\frac{73}{30}$	$\frac{21}{10}$	$\frac{34}{15}$	$\frac{8}{5}$
2223	$\frac{59}{30}$	$\frac{13}{5}$	$\frac{12}{5}$	$\frac{11}{5}$	2	$\frac{51}{20}$	$\frac{41}{20}$	$\frac{32}{15}$	$\frac{79}{30}$	$\frac{23}{10}$	$\frac{37}{15}$	$\frac{9}{5}$
5	$\frac{17}{12}$	$\frac{41}{20}$	$\frac{37}{20}$	$\frac{33}{20}$	$\frac{29}{20}$	2	$\frac{3}{2}$	$\frac{19}{12}$	$\frac{25}{12}$	$\frac{7}{4}$	$\frac{23}{12}$	$\frac{5}{4}$
223	$\frac{23}{12}$	$\frac{51}{20}$	$\frac{47}{20}$	$\frac{43}{20}$	$\frac{39}{20}$	$\frac{5}{2}$	2	$\frac{25}{12}$	$\frac{31}{12}$	$\frac{9}{4}$	$\frac{29}{12}$	$\frac{7}{4}$
23	$\frac{11}{6}$	$\frac{37}{15}$	$\frac{34}{15}$	$\frac{31}{15}$	$\frac{28}{15}$	$\frac{29}{12}$	$\frac{23}{12}$	2	$\frac{5}{2}$	$\frac{13}{6}$	$\frac{7}{3}$	$\frac{5}{3}$
7	$\frac{4}{3}$	$\frac{59}{30}$	$\frac{53}{30}$	$\frac{47}{30}$	$\frac{41}{30}$	$\frac{23}{12}$	$\frac{17}{12}$	$\frac{3}{2}$	2	$\frac{5}{3}$	$\frac{11}{6}$	$\frac{7}{6}$
3	$\frac{5}{3}$	$\frac{23}{10}$	$\frac{21}{10}$	$\frac{19}{10}$	$\frac{17}{10}$	$\frac{9}{4}$	$\frac{7}{4}$	$\frac{11}{6}$	$\frac{7}{3}$	2	$\frac{13}{6}$	$\frac{3}{2}$
4	$\frac{3}{2}$	$\frac{32}{15}$	$\frac{29}{15}$	$\frac{26}{15}$	$\frac{23}{15}$	$\frac{25}{12}$	$\frac{19}{12}$	$\frac{5}{3}$	$\frac{13}{6}$	$\frac{11}{6}$	2	$\frac{4}{3}$
\emptyset	$\frac{7}{6}$	$\frac{9}{5}$	$\frac{8}{5}$	$\frac{7}{5}$	$\frac{6}{5}$	$\frac{7}{4}$	$\frac{5}{4}$	$\frac{4}{3}$	$\frac{11}{6}$	$\frac{3}{2}$	$\frac{5}{3}$	1

Table 21: Negated roots of p for $\alpha A_n \beta$ with an asymmetric lead ordering giving fixed numerator jumps in fixed denominator groups.

C $n < 0$ extrapolated endpoints

All endpoints appear either directly or extrapolated ends at level $n \geq -1$ as shown in [2] where the latter extrapolations at $n = -1$ are carried out. Here we compute extrapolated endpoints appearing at $n \leq -2$ and find that the minimum n where any valid endpoint appears is $n = -10$. Below this, there do not appear to be any valid SCFT endpoints. All structure of the endpoint landscape can thus safely be viewed by considering only $n \geq -10$. Not all extrapolated endpoints occur for both a given fraction formula and in reversed orientation from that of the formula for the isomorphic orbifold family having reversed string order. We refer to endpoints which do as *well-formed*. Counts of the number of endpoints in each extrapolated level appear in Table 22. Level $n = -1$ counts are modified to become 63 if we use the canonical base truncation induced $f(n)$.

Curiously, there is a unique lowest level extrapolated endpoint and a unique lowest level well-formed extrapolated endpoint, namely 29 and 262, respectively. Each supports a unique base and enhancement, these being $\mathfrak{su}(2) \oplus \mathfrak{g}_2 \oplus \mathfrak{e}_8$ on 3221(12) and $\mathfrak{su}(2)^{\oplus 2} \oplus \mathfrak{g}_2^{\oplus 2} \oplus \mathfrak{e}_8$ on 3221(12)1223.

All ($n < 0$)-level extrapolated endpoints are detailed below. Since well-formed extrapolations can be easily determined from the data including non-well formed cases, we confine our listings to the latter. The 27 additional linear endpoints $x_1 \cdots x_r$ not of the form $\alpha A_{n \geq 0} \beta$ for $\alpha \bar{\beta} \in H$ were shown in [2] to occur precisely at level $n = -1$ as *extrapolated endpoints* corresponding to the formulas of Table 1 with $n = -1$. For two reasons, we give all extrapolations for levels $n < -1$ (though no new endpoints arise). First, the breakdowns in orbifold action for linear endpoint families takes place strictly for $-n = 0, 1, 2$,

n	≥ 4	3	2	1	0	-1	-2	-3	-4	-5	-6	-7	≤ -8
#(linear endpts.)	78	78	78	78	77	56	27 [†]	56	45	21	5	1	0
#(all endpts.)	81	82	82	82	81	*	*	...					

Table 22: Number of distinct well-formed extrapolated endpoints at level n . An $n = -2$ ambiguity indicated by ‘†’ arises where we use the convention that q root at $n = -2$ yields the empty endpoint. For branching endpoints, we do not aim to specify negative n counts as indicated by the ‘*’ symbol.

suggesting the structure of these singularities may be of interest. Second, endpoint extrapolations only exist for small $-n$ and hence provide a finite novel combinatorial structure yet to be detailed.

β	7	3222	33	42	6	322	5	4	32222	3	32	\emptyset
α												
22223	22228	22224222	222243	222252	22227	2222422	22226	22225	222242222	22224	222242	2222
6	11	7222	73	82	10	722	9	8	72222	7	72	-
24	29	25222	253	262	28	2522	27	26	252222	25	252	2
33	38	34222	343	352	37	3422	36	35	342222	34	342	3
2223	2228	2224222	22243	22252	2227	222422	2226	2225	22242222	2224	22242	222
5	10	6222	63	72	9	622	8	7	62222	6	62	-
223	228	224222	2243	2252	227	22422	226	225	2242222	224	2242	22
23	28	24222	243	252	27	2422	26	25	242222	24	242	2
7	12	8222	83	92	11	822	10	9	82222	8	82	-
3	8	4222	43	52	7	422	6	5	42222	4	42	-
4	9	5222	53	62	8	522	7	6	52222	5	52	-
\emptyset	-	-	-	-	-	-	-	-	-	-	-	-

Table 23: Level $n = -1$ extrapolated ends.

β	7	3222	33	42	6	322	5	4	32222	3	32	\emptyset
α												
22223	-	222322	2224	223	-	22232	2	22	2223222	222	2223	-
6	45	-	32	422	44	-	43	42	-	3	2	4
24	225	32	-	2222	224	3	223	222	322	-	-	22
33	24	422	5	-	23	42	22	-	4222	-	4	2
2223	-	22322	224	23	-	2232	-	2	223222	22	223	-
5	35	-	22	322	34	-	33	32	-	2	-	3
223	-	2322	24	3	-	232	-	-	23222	2	23	-
23	-	322	4	-	-	32	-	-	3222	-	3	-
7	55	-	42	522	54	2	53	52	-	4	3	5
3	-	-	-	-	-	-	-	-	-	-	-	-
4	25	-	-	222	24	-	23	22	-	-	-	2
\emptyset	-	-	-	-	-	-	-	-	-	-	-	-

Table 24: Level $n = -2$ extrapolated ends.

$\alpha \backslash \beta$	7	3222	33	42	6	322	5	4	32222	3	32	\emptyset
22223	2222226	222222222	22222223	22222232	2222225	222222222	2222224	2222223	22222222222	2222222	22222222	222222
6	526	522222	5223	5232	525	52222	524	523	5222222	522	5222	52
24	2326	2322222	23223	23232	2325	232222	2324	2323	23222222	2322	23222	232
33	3226	3222222	32223	32232	3225	322222	3224	3223	32222222	3222	32222	322
2223	222226	222222222	2222223	2222232	2222225	222222222	2222224	2222223	22222222222	2222222	22222222	222222
5	426	422222	4223	4232	425	42222	424	423	4222222	422	4222	42
223	22226	22222222	222223	222232	22225	2222222	22224	22223	222222222	22222	222222	2222
23	2226	2222222	22223	22232	2225	222222	2224	2223	22222222	2222	22222	222
7	626	622222	6223	6232	625	62222	624	623	6222222	622	6222	62
3	226	222222	2223	2232	225	22222	224	223	2222222	222	2222	22
4	326	322222	3223	3232	325	32222	324	323	3222222	322	3222	32
\emptyset	-	-	-	-	-	-	-	-	-	-	-	-

Table 25: Level $n = -3$ extrapolated ends.

$\alpha \backslash \beta$	7	3222	33	42	6	322	5	4	32222	3	32	\emptyset
22223	-	222223222	-	-	-	222223222	-	2222233	-	2222232	22222322	222223
6	-	532222	-	-	-	53222	-	533	-	532	5322	53
24	-	2332222	-	-	-	233222	-	2333	-	2332	23322	233
33	-	3232222	-	-	-	323222	-	3233	-	3232	32322	323
2223	222236	222232222	2222323	2222332	222235	22223222	222234	222233	222232222	222232	2222322	22223
5	-	432222	-	-	-	43222	-	433	-	432	4322	43
223	22236	22232222	222323	222332	22235	2223222	22234	22233	222322222	22232	222322	2223
23	22236	22232222	222323	222332	22235	2223222	22234	22233	22232222	22232	222322	2223
7	-	632222	-	-	-	63222	-	633	-	632	6322	63
3	236	232222	2323	2332	235	23222	234	233	2322222	232	2322	23
4	336	332222	3323	3332	335	33222	334	333	3322222	332	3322	33
\emptyset	-	-	-	-	-	-	-	-	-	-	-	-

Table 26: Level $n = -4$ extrapolated ends.

$\alpha \backslash \beta$	7	3222	33	42	6	322	5	4	32222	3	32	\emptyset
22223	-	-	-	-	-	-	-	-	-	2222242	-	222224
6	-	-	-	-	-	-	-	-	-	542	-	54
24	-	-	-	-	-	-	-	-	-	2342	-	234
33	-	-	-	-	-	-	-	-	-	3242	-	324
2223	-	222242222	-	-	-	22224222	-	222243	-	222242	2222422	22224
5	-	-	-	-	-	-	-	-	-	442	-	44
223	-	22242222	-	-	-	2224222	-	22243	-	22242	222422	2224
23	-	2242222	-	-	-	224222	-	2243	-	2242	22422	224
7	-	-	-	-	-	-	-	-	-	642	-	64
3	246	242222	2423	2432	245	24222	244	243	2422222	242	2422	24
4	-	342222	-	-	-	34222	-	343	-	342	3422	34
\emptyset	-	-	-	-	-	-	-	-	-	-	-	-

Table 27: Level $n = -5$ extrapolated ends.

$\alpha \backslash \beta$	7	3222	33	42	6	322	5	4	32222	3	32	\emptyset
22223	-	-	-	-	-	-	-	-	-	-	-	222225
6	-	-	-	-	-	-	-	-	-	-	-	55
24	-	-	-	-	-	-	-	-	-	-	-	235
33	-	-	-	-	-	-	-	-	-	-	-	325
2223	-	-	-	-	-	-	-	-	-	222252	-	22225
5	-	-	-	-	-	-	-	-	-	-	-	45
223	-	-	-	-	-	-	-	-	-	22252	-	2225
23	-	-	-	-	-	-	-	-	-	2252	-	225
7	-	-	-	-	-	-	-	-	-	-	-	65
3	-	252222	-	-	-	25222	-	253	-	252	2522	25
4	-	-	-	-	-	-	-	-	-	352	-	35
\emptyset	-	-	-	-	-	-	-	-	-	-	-	-

Table 28: Level $n = -6$ extrapolated ends.

$\alpha \backslash \beta$	7	3222	33	42	6	322	5	4	32222	3	32	\emptyset
22223	-	-	-	-	-	-	-	-	-	-	-	222226
6	-	-	-	-	-	-	-	-	-	-	-	56
24	-	-	-	-	-	-	-	-	-	-	-	236
33	-	-	-	-	-	-	-	-	-	-	-	326
2223	-	-	-	-	-	-	-	-	-	-	-	22226
5	-	-	-	-	-	-	-	-	-	-	-	46
223	-	-	-	-	-	-	-	-	-	-	-	2226
23	-	-	-	-	-	-	-	-	-	-	-	226
7	-	-	-	-	-	-	-	-	-	-	-	66
3	-	-	-	-	-	-	-	-	-	262	-	26
4	-	-	-	-	-	-	-	-	-	-	-	36
\emptyset	-	-	-	-	-	-	-	-	-	-	-	-

(a) Level $n = -7$ endpoints.

$\alpha \backslash \beta$	7	3222	33	42	6	322	5	4	32222	3	32	\emptyset
22223	-	-	-	-	-	-	-	-	-	-	-	222227
6	-	-	-	-	-	-	-	-	-	-	-	57
24	-	-	-	-	-	-	-	-	-	-	-	237
33	-	-	-	-	-	-	-	-	-	-	-	327
2223	-	-	-	-	-	-	-	-	-	-	-	22227
5	-	-	-	-	-	-	-	-	-	-	-	47
223	-	-	-	-	-	-	-	-	-	-	-	2227
23	-	-	-	-	-	-	-	-	-	-	-	227
7	-	-	-	-	-	-	-	-	-	-	-	67
3	-	-	-	-	-	-	-	-	-	-	-	27
4	-	-	-	-	-	-	-	-	-	-	-	37
\emptyset	-	-	-	-	-	-	-	-	-	-	-	-

(b) Level $n = -8$ endpoints.

$\alpha \backslash \beta$	7	3222	33	42	6	322	5	4	32222	3	32	\emptyset
22223	-	-	-	-	-	-	-	-	-	-	-	-
6	-	-	-	-	-	-	-	-	-	-	-	-
24	-	-	-	-	-	-	-	-	-	-	-	-
33	-	-	-	-	-	-	-	-	-	-	-	-
2223	-	-	-	-	-	-	-	-	-	-	-	22228
5	-	-	-	-	-	-	-	-	-	-	-	-
223	-	-	-	-	-	-	-	-	-	-	-	2228
23	-	-	-	-	-	-	-	-	-	-	-	228
7	-	-	-	-	-	-	-	-	-	-	-	-
3	-	-	-	-	-	-	-	-	-	-	-	28
4	-	-	-	-	-	-	-	-	-	-	-	38
\emptyset	-	-	-	-	-	-	-	-	-	-	-	-

(c) Level $n = -9$ endpoints.

$\alpha \backslash \beta$	7	3222	33	42	6	322	5	4	32222	3	32	\emptyset
22223	-	-	-	-	-	-	-	-	-	-	-	-
6	-	-	-	-	-	-	-	-	-	-	-	-
24	-	-	-	-	-	-	-	-	-	-	-	-
33	-	-	-	-	-	-	-	-	-	-	-	-
2223	-	-	-	-	-	-	-	-	-	-	-	-
5	-	-	-	-	-	-	-	-	-	-	-	-
223	-	-	-	-	-	-	-	-	-	-	-	-
23	-	-	-	-	-	-	-	-	-	-	-	-
7	-	-	-	-	-	-	-	-	-	-	-	-
3	-	-	-	-	-	-	-	-	-	-	-	29
4	-	-	-	-	-	-	-	-	-	-	-	-
\emptyset	-	-	-	-	-	-	-	-	-	-	-	-

(d) Level $n = -10$ endpoints.

Table 29: Lowest level extrapolated endpoint tables.

D Lower level endpoint pairing orbits

Linear endpoints appearing *only* as extrapolated endpoints for $n < 0$ have more involved pairing chains moving across levels. This arises since multiple pairings are induced at various $n < 0$ levels which induce further pairings via $n > 0$ -level pairing for small positive n . For example, the self-dual $3A_n3$ family and $33A_n\emptyset$ degenerate to a common endpoint at $n = 0$ to give the only $n = 0$ degeneration of endpoint families. To simplify our presentation, we detail only orbits for the 27 (purely $n < 0$) extrapolated linear endpoints via $n \geq -1$ pairings involving at least on $n = -1$ pair, these appearing in figs. 3–5. These orbits begin to merge upon consideration of $n < -1$ pairings.

N_a matching in T^* pairs often fails to be precise for small and negative n (when T^* pairing chains contain a large number of bases). Having confined our N_a computation to linear bases is at least partially responsible since for short endpoints branching bases are not infrequent. We refer to the chain of endpoints resulting from iterated pairings in each fixed n -level as an n -orbit, e.g. Figure 3b. Longer orbits resulting from iterated pairings across multiple levels since some endpoints appear in more than one level which we denote with the range of n -values to be considered, e.g. $(n \geq -1)$ -orbits as in Figure 3a. We refer to an *orbit* to mean the $(n \geq -1)$ -orbit since all endpoints appear with $n \geq -1$, though these can be strictly smaller than $(n \geq -10)$ -orbits. Orbits appearing in figs. 3–5 illustrate that: (i) orbits have structure beyond mere pairings; (ii) orbits move across levels; and (iii) several distinct $(n = k)$ -orbits arise which may unite as $(n = k')$ -orbits for $k' < k$.

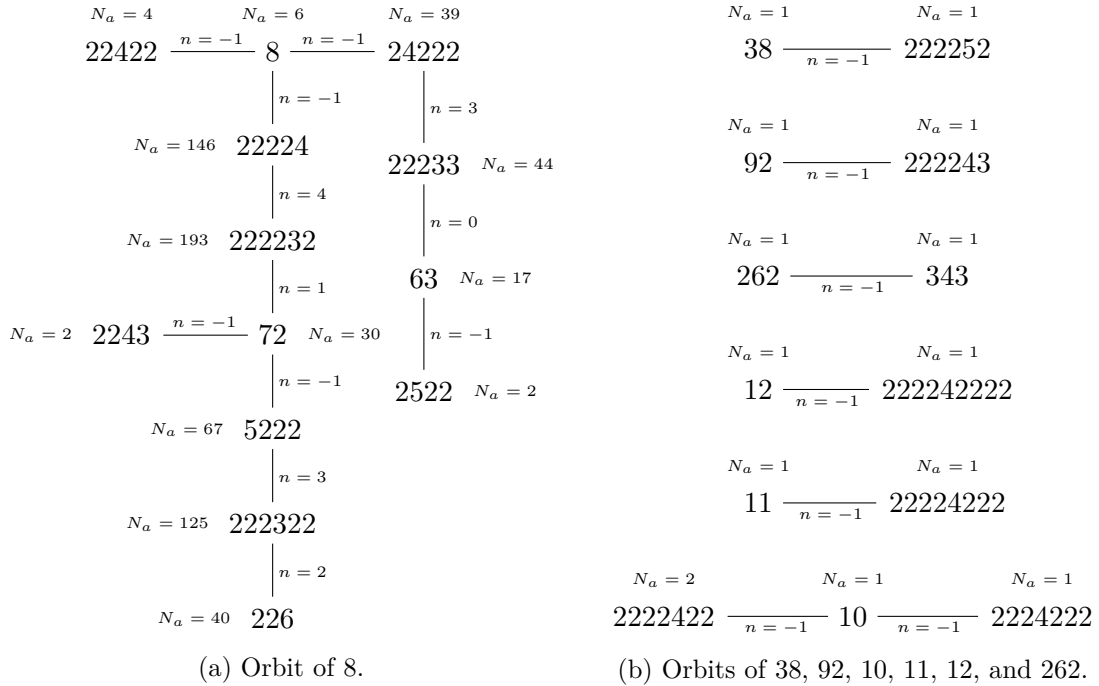


Figure 3: Orbits under $(n \geq -1)$ pairings (I).

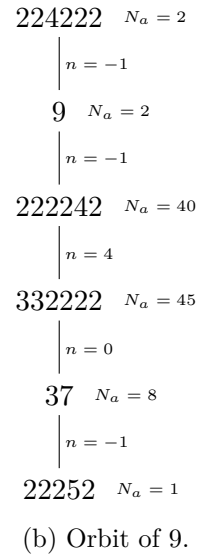
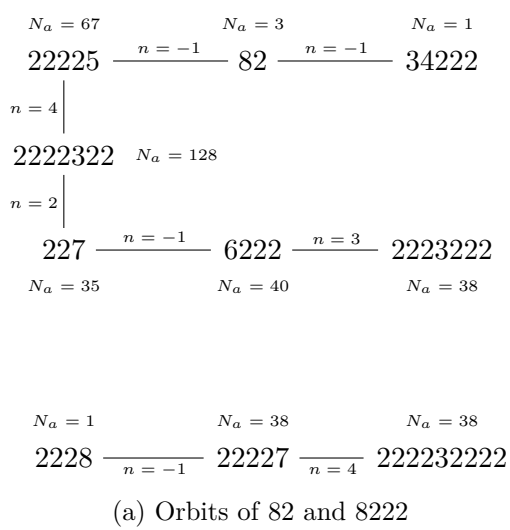


Figure 4: Orbits under $(n \geq -1)$ pairings (II).

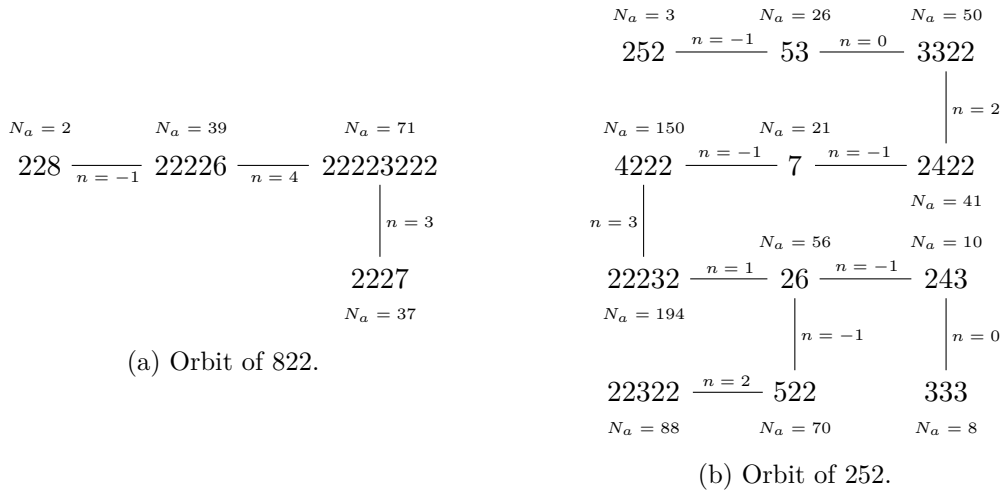


Figure 5: Orbits under $(n \geq -1)$ pairings (III).

References

- [1] Jonathan J. Heckman and David R. Morrison, and Cumrun Vafa. On the Classification of 6D SCFTs and Generalized ADE Orbifolds. *Journal of High Energy Physics*, 05:028, 2014. [Erratum: JHEP06,017(2015)].
- [2] David R. Morrison and Cumrun Vafa. F-theory and $\mathcal{N} = 1$ SCFTs in four dimensions. *Journal of High Energy Physics*, 08:070, 2016.
- [3] Miles Reid. Surface cyclic quotient singularities and Hirzebruch–Jung resolutions. *Unpublished; Manuscript available at <http://homepages.warwick.ac.uk/~masda/surf/more/cyclic.pdf>*, 2012.
- [4] Yuji Tachikawa. Frozen singularities in M and F theory. *Journal of High Energy Physics*, 2016(6):128, 2016.
- [5] Lakshya Bhardwaj, David R. Morrison, Yuji Tachikawa, and Alessandro Tomasiello. The frozen phase of F-theory. *arXiv:1805.09070*, 2018.
- [6] Jonathan J. Heckman, and David R. Morrison, Tom Rudelius, and Cumrun Vafa. Atomic Classification of 6D SCFTs. *Fortschritte der Physik*, 63:468–530, 2015.
- [7] Peter R. Merks. Classifying global symmetries of 6D SCFTs. *To appear in Journal of High Energy Physics*, *arXiv:1711.05155 [hep-th]*, 2018.
- [8] Jonathan Heckman and Tom Rudelius. Top down approach to 6d scfts. *Journal of Physics A: Mathematical and Theoretical*, 2019.
- [9] Robert Daniel Carmichael. *Introduction to the theory of groups of finite order*, volume 19. Ginn Boston, 1937.
- [10] Robert Griess Jr and A Ryba. Finite simple groups which projectively embed in an exceptional lie group are classified! *Bulletin of the American Mathematical Society*, 36(1):75–93, 1999.
- [11] Peter R. Merks. Global Symmetries of Six Dimensional Superconformal Field Theories. *University of California, Santa Barbara Doctoral Thesis*, 2017.